ORNL-3615
UC-34 – Physics
TID-4500 (29th ed.)

THE YIELD OF ELASTICALLY SCATTERED 17 TO 21 MeV NEUTRONS FROM THE REACTION $C^{12}(n,n)C^{12}$

Marvin Vernon Harlow, Jr.

OAK RIDGE NATIONAL LABORATORY
operated by
UNION CARBIDE CORPORATION
for the
U.S. ATOMIC ENERGY COMMISSION

ORNL-3615

Contract No. W-7405-eng-26

Physics Division

THE YIELD OF ELASTICALLY SCATTERED 17 TO 21 MeV NEUTRONS FROM THE REACTION $C^{12}(n,n)C^{12}$

Marvin Vernon Harlow, Jr.

(Submitted as a dissertation to the Graduate School of the University of Texas in partial fulfillment of the requirements for the degree of Doctor of Philosophy)

JUNE 1964

OAK RIDGE NATIONAL LABORATORY
Oak Ridge, Tennessee
operated by
UNION CARBIDE CORPORATION
for the
U.S. ATOMIC ENERGY COMMISSION

PREFACE

The preliminary experiments and the development of most of the experimental techniques and apparatus for the work reported in this dissertation, were carried out at the University of Texas. In June 1962, the work was moved to Oak Ridge National Laboratory (ORNL) where the data used in this thesis were taken and analyzed.

It is with great pleasure that we thank Professor B. B. Kinsey for suggesting this dissertation problem and for his invaluable help and continuing interest in the work at the University and that done at ORNL. We also wish to thank him for making the arrangements for the move to ORNL.

The author wishes to take this opportunity to thank the entire staff of the High Voltage Laboratory of ORNL for their interest, their willing assistance, and for their many helpful comments and suggestions. In particular, we most earnestly thank Dr. R. L. Robinson for his assistance with the experimental work and for reading and correcting the many drafts of this dissertation. Dr. R. W. Lamphere is due our special thanks for making available his double foil gas target and for instructing us in its use. We are indebted to Dr. H. B. Willard for his critical reading of Chapter IV, Dr. F. G. Perey for making available his optical model computer code, and Dr. J. A. Biggerstaff for his constructive criticism of many of the computer codes which were developed and used. We would also like to thank Drs. J. K. Dickens and T. Tamura for making available preprints of their proton data and theoretical work, respectively. We are grateful to Drs. P. H. Stelson and F. K. McGowan for their help during the early part of the work at ORNL.

We wish to acknowledge the very able job done by C. W. Williams in designing and developing the version of the Forte circuit which we used. Also the help of C. W. Nestor in the development of some of the computer codes is gratefully acknowledged. We wish to express our appreciation to Althea Stooksbury for her competent typing of the manuscript.

Last, but not least, we most sincerely thank Dr. J. L. Fowler for his interest in our work and for his support of it. The author is grateful to the Oak Ridge Institute of Nuclear Studies for a graduate fellowship.

TABLE OF CONTENTS

CHAPTER I

INTRODUCTION

Several years ago Kinsey[1] reported a resonance in the yield of elastically scattered protons[2] from C^{12} at a proton energy of 22.5 MeV. Dickens[3] recently confirmed and studied this resonance more extensively. This resonance corresponds to an excitation of 22.7 MeV in the compound nucleus[4] N^{13} which is formed by a proton plus C^{12}. If we assume that there is a similar resonance at an excitation energy of 22.7 MeV in C^{13}, which is the compound nucleus formed by a neutron plus C^{12}, then it follows that 19.3 MeV neutrons would be required to produce such a resonance.[5] This dissertation deals with the search for this neutron resonance. Measurements were made of the differential elastic cross section as a function of energy at six scattering angles and the total cross section as a function of energy for 17.2 to 21 MeV neutrons on C^{12}.

The differential elastic cross sections determined by Dickens and the data taken by Kinsey are shown in Figure 1.1. The 60° data are in relative units. For the other data in the figure, the differential cross section is in millibarns per steradian in the center of mass system; the

---

[1] B. B. Kinsey, Phys. Rev. 99, 332 (1955)

[2] Elastically scattered protons are protons which have been scattered suffering no loss in energy in the center of mass coordinate system.

[3] J. K. Dickens, Ph.D Dissertation, University of Southern California, 1962; J. K. Dickens, D. A. Haner, and C. N. Waddell, Phys. Rev. 132, 2159 (1963)

[4] N. Bohr, Nature 137, 344 (1936)

[5] E. C. Monahan, M.A. Thesis, University of Texas, 1961, p. 1

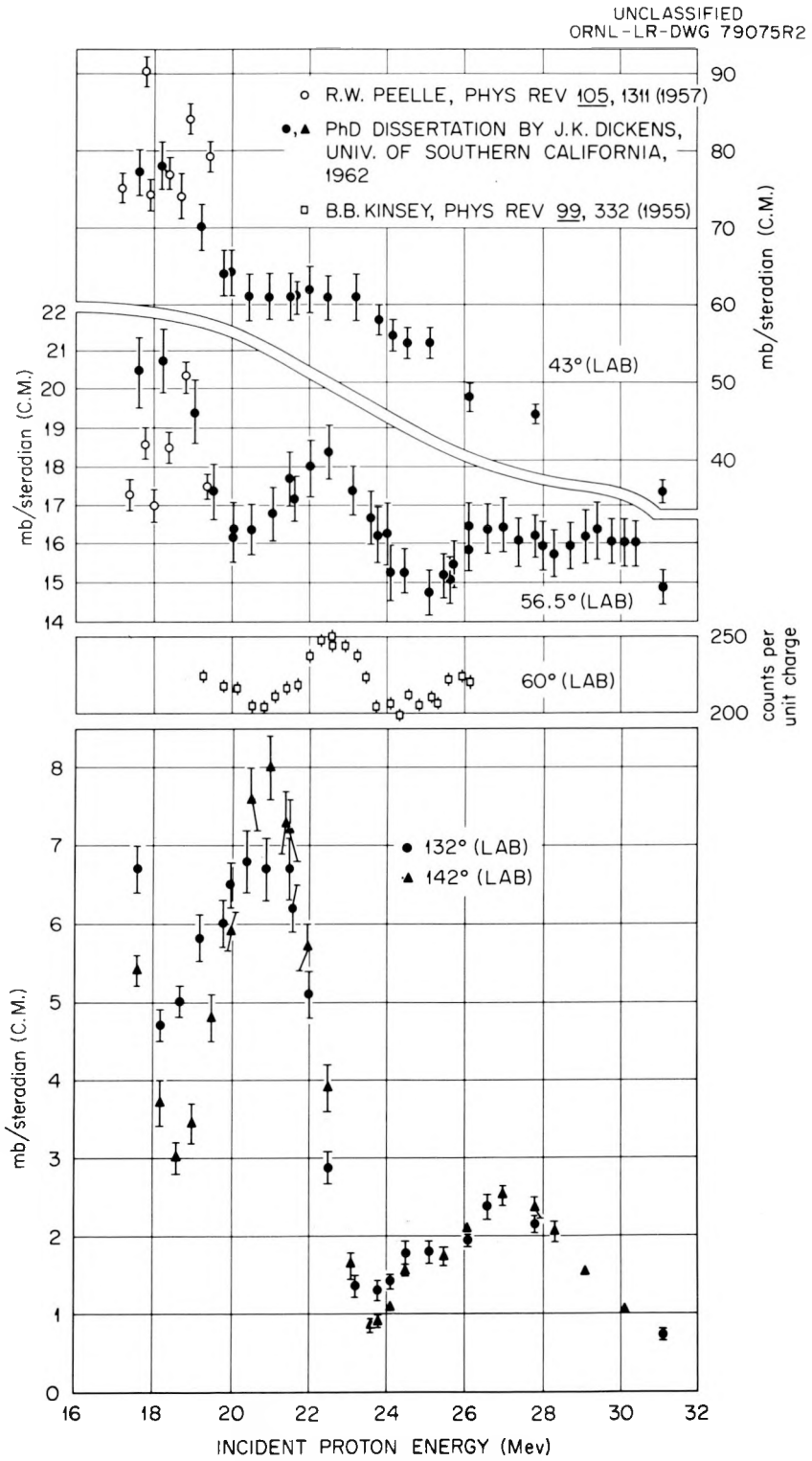

Figure 1.1. Differential Cross Section for Elastic Scattering of Protons by C^{12} Plotted as a Function of Proton Energy.

scattering angle and the incident proton energy are in the laboratory system. If we assume that the proton data in the figure between 19.5 and 24 MeV are a reliable qualitative guide to what one might expect to find for the differential elastic cross section of neutrons for C^{12} between 17.2 and 21 MeV, then there should be a resonance at 19.3 MeV at scattering angles ranging from 43° to about 60°. At these angles this resonance should have a total width at half maximum of about 2 MeV and a peak cross section that is about 12 percent greater than the non-resonant[6] cross section. As in the case of the proton data,[7] the resonance should appear at scattering angles around 130° to 140° as a very rapid change in the differential cross section, possibly by a factor of 7, over an energy interval of 2 MeV.

The total cross section, σ_T, is related to the differential elastic cross section by the equation

$$\sigma_T = 2\pi \int_0^{\pi} \sigma(\theta)\sin\theta \, d\theta + \sigma_{NE}, \qquad (1.1)$$

where $\sigma(\theta)$ is the differential elastic cross section and σ_{NE} is the total non-elastic cross section. If we assume that σ_{NE} is constant in the region of 19.3 MeV, then the total cross section should exhibit a resonance at 19.3 MeV if there is a resonance in $\sigma(\theta)$ at this energy. The total cross section was measured in the neutron energy range of 17.2 to 21 MeV since precise data were not available.

---

[6] The non-resonant cross section is the cross section upon which the resonance is superimposed.

[7] T. Tamura and T. Terasawa (submitted to Phys. Letters for publication)

In the present work the differential elastic cross section was measured using ring geometry,[8] a scintillation neutron detector, and a beam of neutrons which was produced by deuterons from the ORNL 5.5 MV Van de Graaff accelerator. The differential cross section was calculated from experimental parameters and from the measured value of the scattering ratio R at each value of incident neutron energy and at each scattering angle. R is defined as the ratio of the scattered neutron intensity divided by the direct neutron intensity where both the scattered and the direct intensities have been corrected for background.

The total cross section was calculated at each neutron energy from a transmission which was measured by a conventional transmission experiment.[9] The transmission is defined as the ratio of the neutron intensity attenuated by the sample divided by the direct neutron intensity. The measurement was carried out with essentially the same apparatus and neutron source as were used for the differential cross section experiment.

The experimental aspects of the two experiments are discussed in Chapters II and III. We follow this discussion with the calculation of the differential cross section in Chapter IV and the calculation of the total cross section in Chapter V. Chapter VI concludes the dissertation.

---

[8] W. D. Whitehead and S. C. Snowdon, Phys. Rev. 92, 114 (1953); M. Walt, Fast Neutron Physics, Part II, eds. J. B. Marion and J. L. Fowler (New York: Interscience Publishers, Inc., 1963), p. 1033

[9] D. W. Miller, Fast Neutron Physics, Part II, eds. J. B. Marion and J. L. Fowler (New York: Interscience Publishers, Inc., 1963), p. 985

In it we compare the proton differential elastic cross section[10,11] with the neutron differential cross section, as calculated in Chapter IV, and the total cross section, calculated in Chapter V, with data taken by another group.

---

[10] B. B. Kinsey, op. cit.

[11] J. K. Dickens et al., op. cit.

CHAPTER II

EXPERIMENTAL APPARATUS

2.1 Introduction

Essentially the same apparatus was used for both the differential cross section experiment and the total cross section experiment. We first discuss each of the pieces of the equipment common to both of the two experiments: the detector, the monitor, the target, and the support stand for the detector, for the sample, and for the attenuation bar. We conclude the chapter with discussions of the samples and geometries used in each of the two experiments.

2.2 The Neutron Detector and Associated Electronics

The neutron detector was a scintillation detector utilizing pulse shape discrimination to separate proton recoil pulses from pulses due to electrons arising from the interaction of gamma rays with the stilbene crystal. A block diagram of the detector and the associated electronics is shown in Figure 2.1. The detector was made up of the 1 in. X 1 in. stilbene crystal, a 1 in. diameter by 3.5 in. long lucite light pipe, a 6810A photomultiplier tube, a tube base, and emitter followers. The associated electronics was divided into a linear channel, a slow-component channel, a slow coincidence circuit, display electronics, and two scalers.

For the differential cross section experiment and, incidentially, for the total cross section experiment, the detector had to have good energy resolution. Since energy resolution of the detector was strongly dependent upon the quality of the stilbene crystal and on the way in which it was

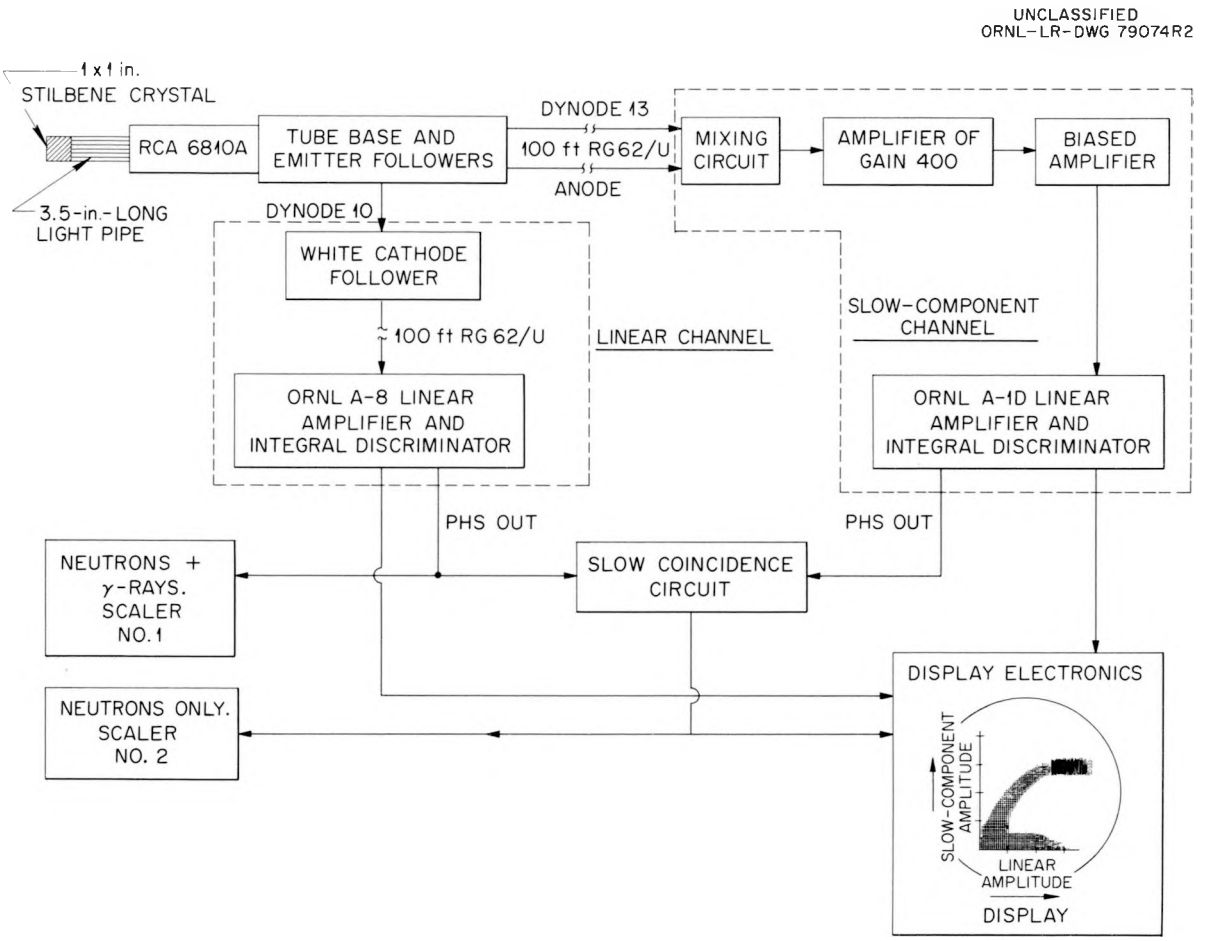

Figure 2.1. Block Diagram of the Detector Electronic System.

mounted, a 1 in. X 1 in. stilbene crystal, which was transparent and free of cracks was used. It was carefully mounted in the following manner. After being wrapped in aluminum foil and taped with plastic tape, the crystal and the light pipe were placed in a light-tight housing made of thin wall brass. The housing supported the crystal and the light pipe in a position such that the cylindrical axes of the crystal and the light pipe were identical with the cylindrical axis of the photomultiplier tube. The crystal was pressed against the light pipe, and the light pipe was pressed against the photocathode by a disk spring located between the end of the housing and the front face of the stilbene crystal. Optical coupling of the crystal and the photomultiplier tube to the light pipe was made with silicon vacuum grease.

The principle of operation of the detector is reasonably straightforward. If a neutron incident on the organic stilbene crystal collides with a hydrogen nucleus in the crystal, a recoil proton is produced. We can neglect the effects of a neutron collision with a carbon nucleus. If the recoil proton is completely absorbed by the stilbene crystal, a light pulse is produced which has an amplitude that is a function of the energy of the recoil proton. This light pulse is transmitted through the light pipe to the photocathode of the photomultiplier tube and there produces photoelectrons. The multiplier chain of the photomultiplier tube linearly amplifies the initial photoelectron current by a factor of about 10 million to produce a current pulse which can be adequately handled by conventional vacuum tube or transistor fast pulse techniques. Gamma rays interacting with the stilbene crystal give rise to electrons

which, when completely absorbed by the crystal, result in light pulses which have amplitudes proportional to the energy of the electrons.

The voltage divider network of the photomultiplier tube was designed to allow a current pulse in the photomultiplier tube to be sampled at dynodes 10 and 13 and at the anode. The pulse from dynode 10 had an amplitude proportional to the light output from the stilbene crystal. It was fed into the A-8 linear amplifier in the manner shown in Figure 2.1. The output of the A-8 amplifier went to the display electronics and to a multichannel analyzer used for calibration purposes. The integral discriminator of the amplifier, which was used as the detector bias control, was connected to scaler number one and to the slow coincidence circuit. Data taken on scaler number one were used to monitor the overall performance of the detector electronics system by showing up any failures which might have occurred in the pulse shape discrimination circuit or in scaler number two.

The total and the differential cross sections calculated from the data taken with scaler number one and number two agreed within statistics in all cases except for those differential cross sections taken at 124° and 139°. For these two angles, the detector bias had to be set below a neutron energy of 13 MeV which allowed gamma rays absorbed by the stilbene crystal to be recorded by scaler number one. These calculated differential cross sections were about 40 percent greater than those calculated from the scaler number two data. Hence, the pulse shape discrimination circuit did not play an important role except for measurements taken at these two angles.

A pulse produced by a gamma ray and one produced by a neutron are

similar to the extent that they can both be decomposed into a fast component having a decay time of 6.2×10^{-9} sec and a slow component having a decay time of 370×10^{-9} sec.[1] For both types of pulses, more than 90 percent of the charge is contained in the fast component,[2] where the areas are defined in Figure 2.2a. For a gamma ray pulse and a neutron pulse of equal amplitudes, the amplitude of the slow component of the neutron pulse is 1.8 times that of the gamma ray pulse.[3] The pulse shape discrimination circuit that was used took advantage of this difference in the slow component amplitudes to separate neutron pulses from gamma ray pulses.

This pulse shape discrimination circuit was essentially a Forte circuit[4] which was modified by removing the adjustable circuit elements from the tube base and relocating them a safe distance from the neutron beam originating from the gas target. The adjustable circuit elements were the mixer, the amplifier of gain 400, and the biased amplifier. These circuit elements are shown in the block diagrams of Figures 2.1 and 2.2. This modified Forte circuit was capable of discriminating between gamma rays and neutrons for electron energies greater than approximately 70 keV (neutron energies of 620 keV).

---

[1] R. B. Owen, Proceedings of the International Symposium on Nuclear Electronics, Vol. I, (Vienna: International Atomic Energy Agency, 1959), p. 27

[2] F. W. K. Firk, Fast Neutron Physics, Part II, eds. J. B. Marion and J. L. Fowler, (New York: Interscience Publishers, Inc., 1963), p. 2237

[3] R. B. Owen, op. cit.

[4] M. Forte, A. Konsta, and C. Maranzana, Proceedings of the Conference on Nuclear Electronics, Vol. II, (Vienna: International Atomic Energy Agency, 1962), p. 277

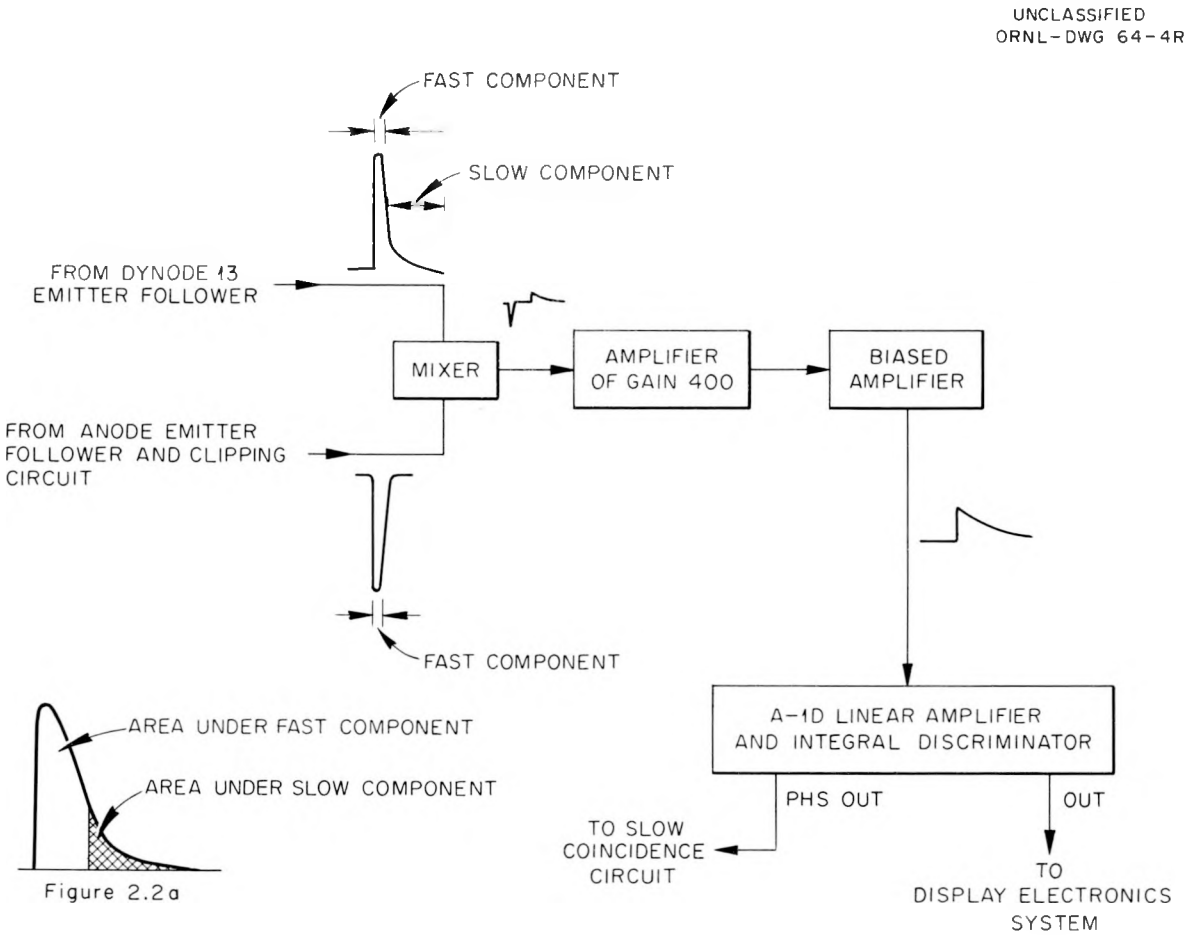

Figure 2.2. Pulse Mixing in the Forte Circuit.

The function of the Forte circuit was to remove the fast component from the dynode 13 pulse and to amplify the remaining slow component. These two operations are shown schematically in Figure 2.2. The slow component of the anode pulse was eliminated by differentiating the pulse with a resistor, capacitor differentiation network and by removing the resulting positive overshoot with a biased "off" emitter follower. The dynode 13 pulse and the clipped anode pulse were then combined in the mixer circuit in such a way that the fast component from the dynode 13 pulse was removed.

A positive sum pulse (called the slow-component pulse) having an amplitude proportional to the slow component of the unmixed dynode 13 pulse was produced by the mixer circuit. The circuit also served to approximately normalize the slow-component pulse to the total pulse height of the unmixed dynode 13 pulse. There was a negative spike preceding the slow-component pulse which was caused in the mixing circuit by a slight difference in the shape of the fast components of the unmixed dynode 13 pulse and the clipped anode pulse. This spike was removed from the slow-component pulse by the gain of 400 amplifier and the biased amplifier shown in Figures 2.1 and 2.2. After being amplified by the A-1D amplifier, the slow-component pulse was fed into the display electronics. The integral discriminator of the A-1D amplifier was fed into the slow coincidence circuit.

The mixing circuit was so adjusted that the slow-component pulse height of a gamma ray pulse was no more than one half the slow-component pulse height of a neutron pulse having a total amplitude equal to that of the gamma ray for neutron energies greater than 8 MeV. The display

electronics system was used to indicate when the optimum adjustment of the Forte circuit had been reached.

Since the display system was an analogue three dimensional pulse height analyzer, its operation is more easily understood if one assigns an x and a y coordinate to each light pulse detected by the photomultiplier tube. We let the x coordinate be the total pulse height of a pulse. The output from the A-8 amplifier shown in Figure 2.1 is proportional to this total pulse height. The amplitude of a slow-component pulse obtained from the A-1D amplifier of Figure 2.1 is taken to be the y coordinate. For every pulse having an x and a y coordinate large enough to satisfy the coincidence conditions of the slow coincidence circuit, a dot appeared on the display oscilloscope. The coordinates of the location of the dot on the oscilloscope are proportional to the x and y coordinates, respectively. The third dimension of the display system was the number of pulses having a particular set of x and y coordinates which occurred in a given interval of time. A qualitative indication of this number was obtained from the intensity of the dot on the long persistent screen of the oscilloscope. Typical displays for an optimum adjustment of the mixer circuit are shown in Figures 2.1 and 3.3.

Once the mixing circuit had been adjusted to give an optimum display, the integral discriminators of the A-1D and the A-8 amplifiers were set. The procedure for setting these discriminators is described in detail in Section 3.4. It is sufficient to say here that the discriminators were set so that only proton recoil pulses having an energy greater than that corresponding to the discriminator setting of the A-8 amplifier could trigger the slow coincidence circuit shown in Figure 2.1.

The output pulses of the slow coincidence circuit were counted by scaler number two and were also used to gate the display electronics system.

A spectrum of proton recoil pulses resulting from the bombardment of the stilbene crystal of the detector with a direct beam of 20.87 MeV monoenergetic neutrons is shown in Figure 2.3. Spectra similar to this one were used to calibrate the detector bias in terms of neutron energy. The spectrum was obtained with a multichannel pulse height analyzer which was connected to the output of the A-8 amplifier shown in Figure 2.1 and which was gated with the output of the slow coincidence circuit. The spectrum was taken after the mixer circuit had been adjusted to an optimum setting. It is reasonably flat; the counts per channel change about 15 percent over the energy interval of 11.8 to 20.9 MeV. The channel number at the half maximum of the forward edge of the spectrum (that part of the spectrum around channel 85) corresponds to a neutron energy of 20.87 MeV. The bias edge of the spectrum results from the integral discriminator of the A-8 amplifier shown in Figure 2.1. Calibration of the bias edge in terms of neutron energy is discussed in Section 3.3.

2.3 The Neutron Monitor and Associated Electronics

In both the differential cross section experiment and the total cross section experiment, only a relative measurement of the neutron intensity from the target was required. This relative flux measurement was made with the monitor counter which was placed at a fixed position 9 in. from the target. The monitor was a proton recoil scintillation detector of conventional design. The 1 cm X 1 cm plastic scintillator that was used was small enough to limit the maximum detectable electron

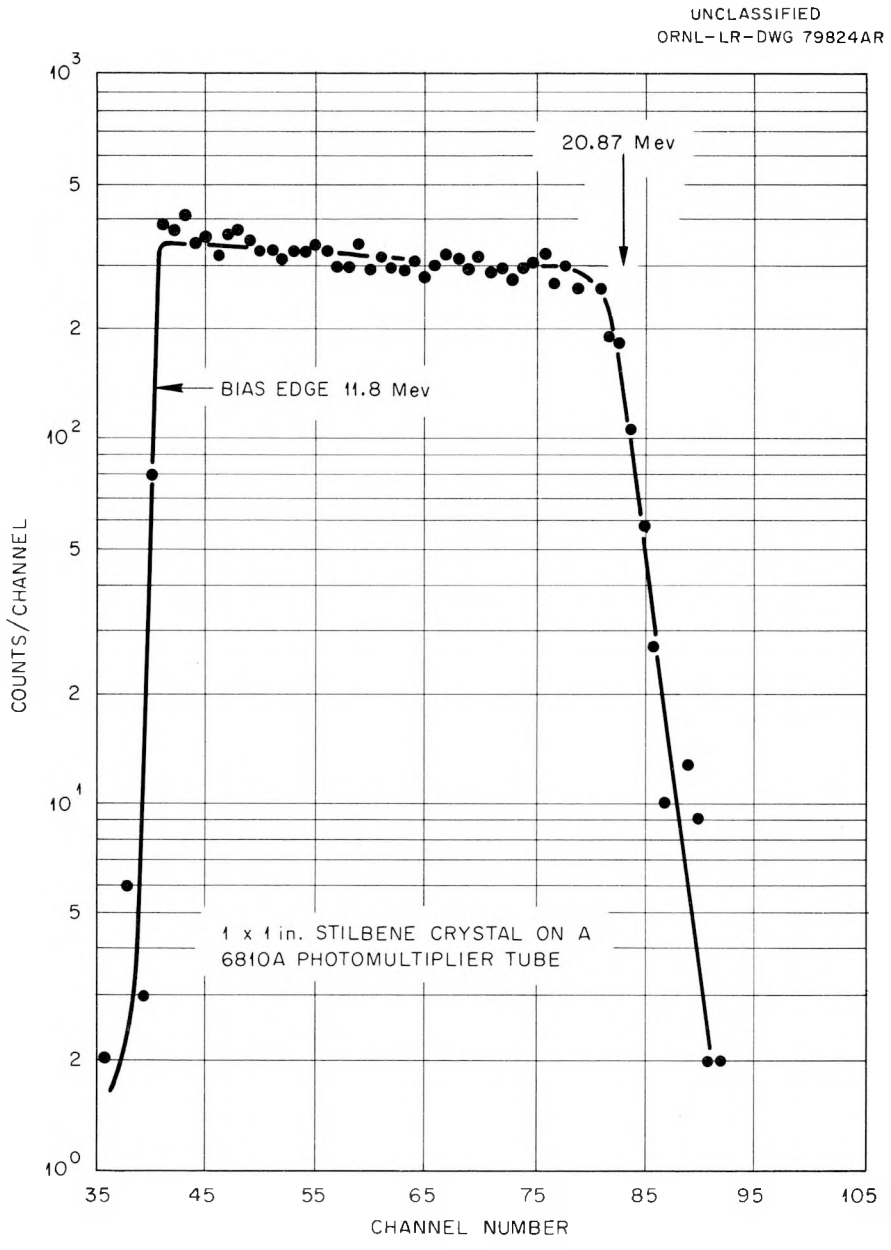

Figure 2.3. Proton Recoil Spectrum of 20.87 MeV Neutrons from the $T(d,n)He^4$ Reaction.

pulse due to a gamma ray to about 4 MeV and yet large enough to have adequate sensitivity to 17 to 21 MeV neutrons.

Figure 2.4 shows the electronic circuitry associated with the monitor which was of conventional design. The integral discriminator of the A-8 amplifier was set above the maximum possible pulse height of electrons resulting from gamma ray interactions (i.e., 4 MeV) in the crystal. With this setting, the monitor would record only neutrons from the target produced by the $T(d,n)He^4$ reaction of the target. Neutrons from the reaction $D(d,n)He^3$ were not recorded by the monitor scaler because the maximum proton recoil pulse height due to these neutrons was below the integral discriminator setting of the A-8 amplifier.

Figure 2.5 shows a typical neutron spectrum which was taken to check the performance of the monitor counter and to serve as a guide for setting the integral discriminator. The spectrum was obtained by connecting the output of the A-8 amplifier of Figure 2.4 to the input of the multichannel analyzer and gating the analyzer with the integral discriminator of the amplifier.

2.4 The Tritium Gas Target

The source of neutrons for both experiments was the $T(d,n)He^4$ reaction. The tritium was contained in a double foil gas target and was bombarded with a deuteron beam from the Van de Graaff accelerator. For the case of a 5 μa deuteron beam having an energy of 3 MeV at the center of the tritium gas cell (3 cm long containing 0.43 atm of tritium), the neutron yield from the target was 2.3×10^8 neutrons per second. This

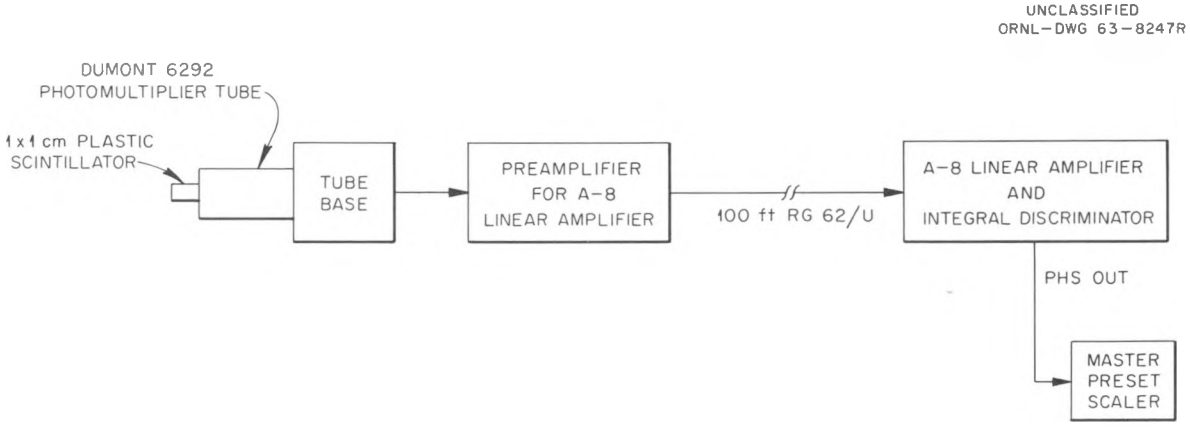

Figure 2.4. Block Diagram of the Monitor Electronic Circuitry.

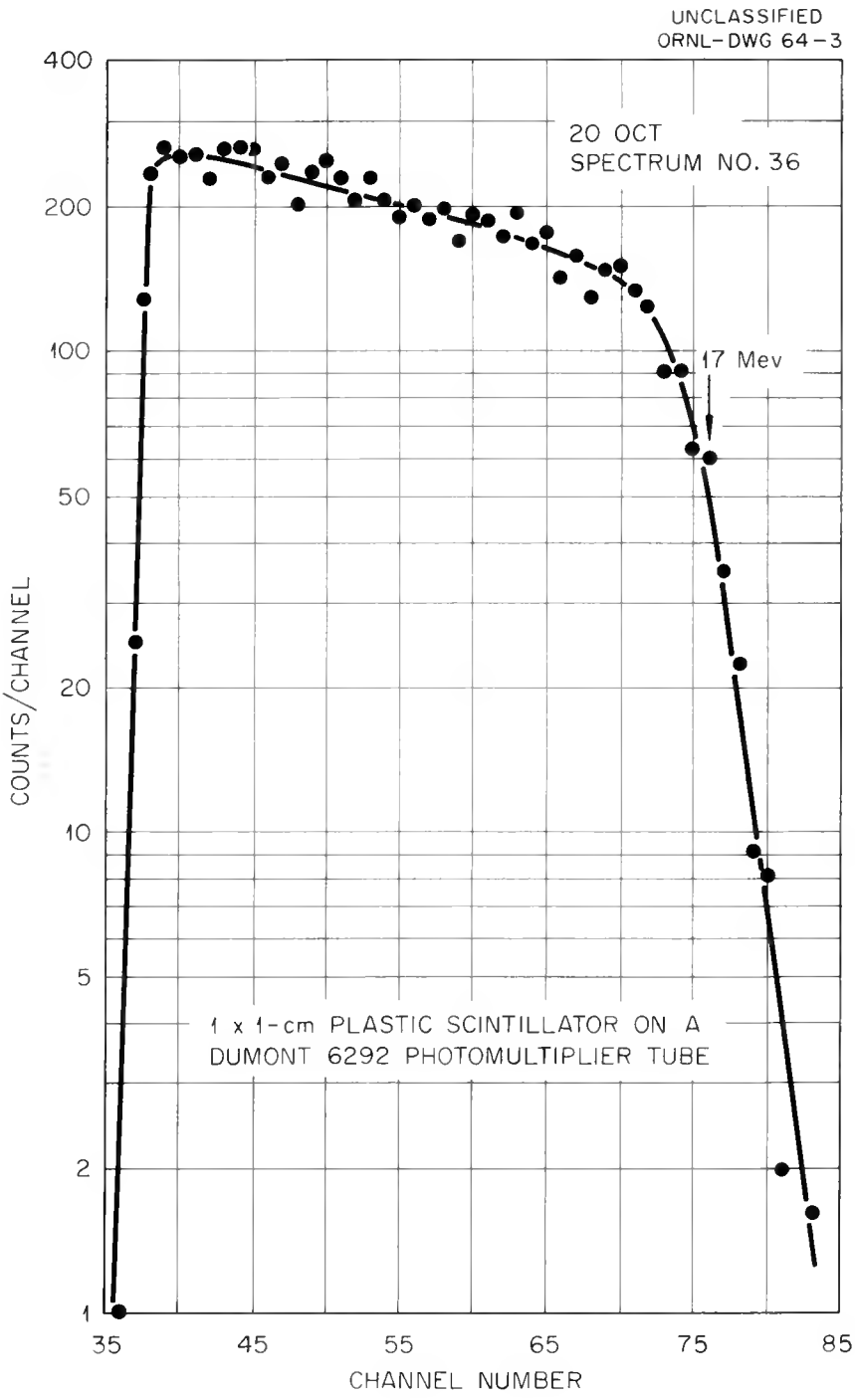

Figure 2.5. Recoil Proton Spectrum for the Monitor Counter.

neutron yield is about 14 times that which one would obtain for a zirconium tritide target of equivalent thickness.

A schematic diagram of the double foil gas target is shown in Figure 2.6. It can be operated at a maximum proton beam current of 22 μa, which is about a factor of 10 greater than the maximum proton beam current which can be handled by a single foil gas target.[5] A stream of unrefrigerated helium gas was used to cool the two one mil thick nickel foils.[6] The helium cooling gas was recirculated through a closed gas handling system that contained a compressor and a network of filters for filtering the gas before it re-entered the cooling cell.

Figure 2.7 is a schematic diagram of the vacuum system between the analyzing magnet of the accelerator and the tritium gas cell. The electrostatic quadrupole lens shown in the figure was placed midway between the analyzing magnet and the target and was used to focus the beam on the gas target. Isolation of the target area from the background produced in the neighborhood of the analyzing magnet was accomplished by the two foot thick concrete wall. When the first foil of the target ruptured, the fast shutoff valve closed, thus preventing the accelerator vacuum system from being spoiled by the flow of helium cooling gas. The target was supported in the position shown in Figure 2.7 by supporting members fastened to the wall and the ceiling of the room. These

---

[5] R. W. Lamphere (private communication)

[6] The foils were grade C foils purchased from the Cromium Corporation of America, Waterbury, Connecticut.

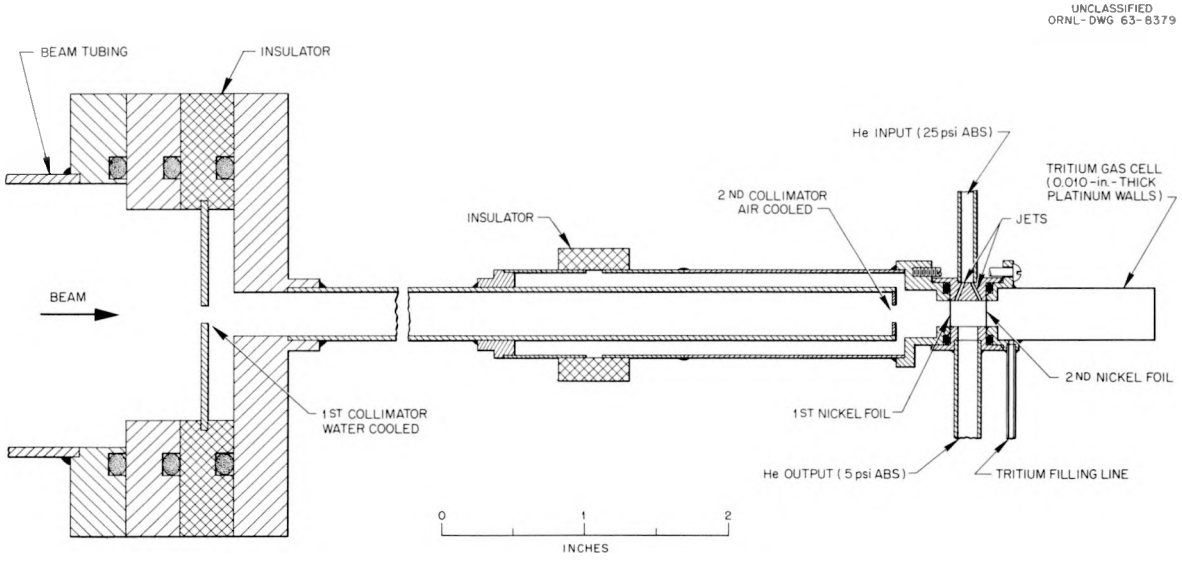

Figure 2.6. Schematic Diagram of the Double Foil Gas Target.

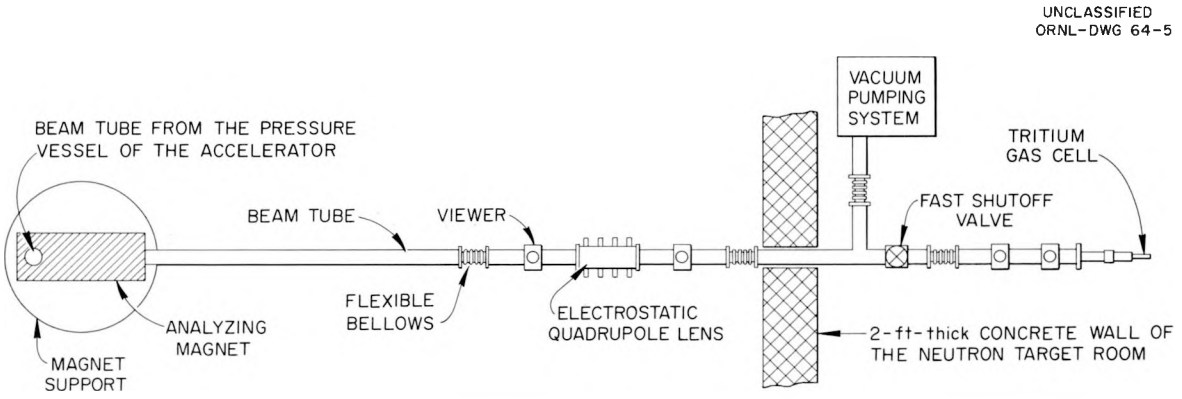

Figure 2.7. A Sketch of the Top View of the Vacuum System Between the Analyzing Magnet and the Tritium Gas Cell.

supporting members could be adjusted so that the target could be moved a small amount in any direction and then locked in the desired position.

2.5 The Support Stand for the Detector, Sample and the Attenuation Bar

Apparatus for supporting the detector, sample and the attenuation bar was essentially the same for both the differential cross section and the total cross section experiments. A rigid platform made of duralumin having a horizontal surface 3 in. wide and 63 in. long was the main part of the apparatus.[7] This platform could be rotated in a horizontal plane about a vertical axis which passed through both the rotation point of the platform and the center-point of the gas target cell. The angle of rotation, called the platform rotation angle, was defined by the angle between the center-line of the horizontal surface of the platform and the axis of the deuteron beam. It was always fixed at zero degrees except during the calibration of the detector bias.

The detector, sample and the attenuation bar were rigidly supported approximately 12 in. above and directly over the center-line of the platform by legs made of thin wall brass tubing. These legs were fastened to the platform in such a way that the position of a piece of supported apparatus could be adjusted in a horizontal plane in a direction perpendicular to the center-line of the platform or in a direction along the center-line of the platform. They were also designed to permit a certain amount of vertical adjustment.

---

[7] For a discussion of the platform and the background of neutrons scattered from it, see E. C. Monahan, op. cit.

2.6 The Samples and the Experimental Geometries

Samples used in both of the experiments were composed of natural carbon which contains 99 percent C^{12} and one percent C^{13}. Since the total cross section of C^{13} (approximately 1.6 barns between 15 and 19 MeV[8]) is about the same as that for C^{12}, the natural carbon samples that were used were treated as composed entirely of C^{12}. Table 2.1 gives the results of the analysis of the carbon used for samples for the two experiments. We see from the table that ATJ grade reactor graphite and electrode graphite are essentially identical from the point of view of impurities, and that each is of high purity.

The geometrical axis of each experiment was defined by the extension of the direction of the deuteron beam beyond the end of the tritium gas cell. Each of the experimental geometries required that the cylindrical axes of the detector, the sample and the attenuation bar (when used) correspond to the geometrical axis of the experiment. As a matter of convenience, the center-line of the supporting platform was aligned to be parallel to the geometrical axis and to be contained in the same vertical plane as the geometrical axis. The position of the monitor was the same for both experiments: it was 9 in. from the center of the tritium gas cell and at an angle of 55 degrees with respect to the direction of the deuteron beam.

The experimental geometry used for the differential cross section experiment is shown in Figure 2.8. It is called ring geometry because

---

[8] H. O. Cohn, J. K. Bair, and H. B. Willard, Phys. Rev. 122, 534 (1961)

Table 2.1

SEMIQUANTITATIVE SPECTROCHEMICAL ANALYSIS OF THE SAMPLES

Analysis done by ORNL Spectrochemical Laboratory
Carbon sample No. 1 - ATJ Pile Grade Graphite
Carbon sample No. 2 - Electrode Graphite cut from stock piece of electric furnace electrode.

SYMBOLS

A: 10-100% C: 0.1-1% E: 0.001-0.01%
B: 1-10% D: 0.01-0.1% F: 0.0001-0.001%
-: Sought; not found (See limit of detection below)

FILM NO. 8162
DATE 6-26-63
BY C. A. Pritekard
FOR J. W. Johnson

Numerical results below are considered accurate to within ± 30%

Element	Limit of Detection (%) for these Samples	Carbon Sample No. 1	Carbon Sample No. 2	Element	Limit of Detection (%) for these Samples	Carbon Sample No. 1	Carbon Sample No. 2
Ag	.0003	-	-	Ni	.003	-	-
Al	.006	-	-	P	.12	-	-
As	.04	-	-	Pb	.02	-	-
Au	.001	-	-	Pd	.004	-	-
B	.002	-	-	Pt	.002	-	-
Ba	.18	-	-	Ru	.02	-	-
Be	.0003	-	-	Sb	.008	-	-
Bi	.002	-	-	Si		E	E
Ca		E	E	Sn	.007	-	-
Cd	.01	-	-	Sr	.05	-	-
Co	.002	-	-	Ta	.08	-	-
Cr	.001	-	-	Te	.05	-	-
Cu	.0002	-	-	Th	.14	-	-
Fe		F	E	Ti		D	E
Ga	.03	-	-	Tl	.13	-	-
Ge	.004	-	-	U	.22	-	-
Hg	.006	-	-	V	.005	-	D
K	1.2	-	-	W	.11	-	-
Li	.05	-	-	Zn	.03	-	-
Mg		F	F	Zr	.003	-	-
Mn	.003	-	-	Nb	.05	-	-
Mo	.003	-	-				
Na	.15	-	-				

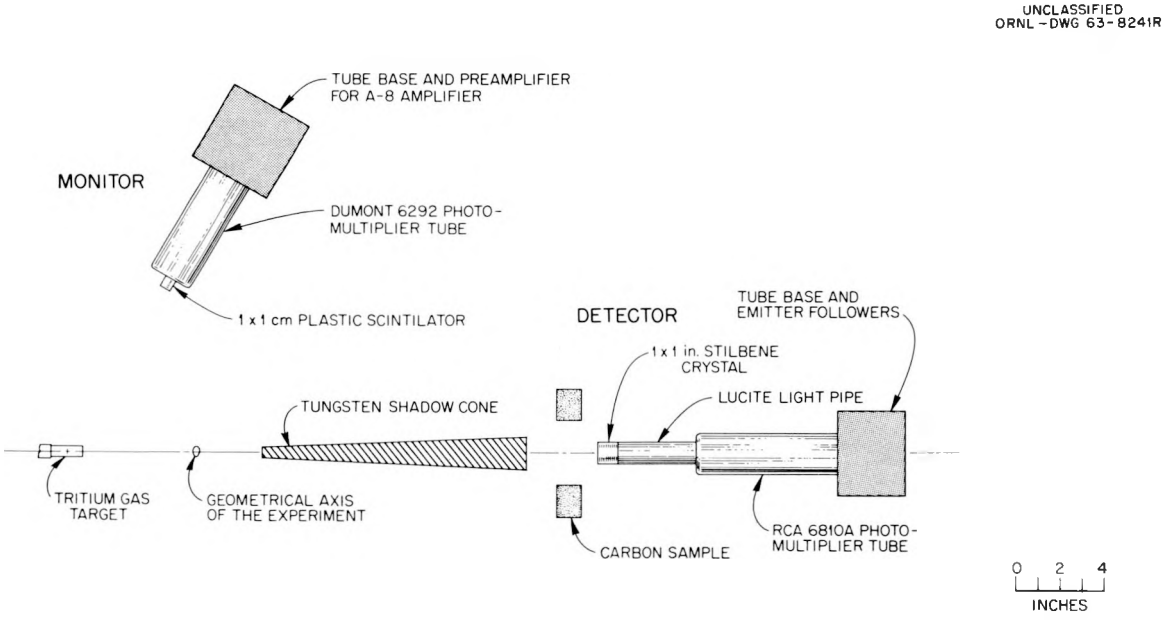

Figure 2.8. Schematic Diagram of the 60° Geometry Used for the Differential Cross Section Experiment. Cross-Sectional View Taken in a Horizontal Plane.

the carbon sample was in the shape of an annulus. Ring geometry was chosen for the experiment because a much larger sample could be used than in the case of cylindrical geometry or slab geometry. The geometrical set-up and the distances for the October 1962 and February 1963 runs on the accelerator are summarized in Table 2.2. D_1 denotes the distance between the center of the target and the center of the cross sectional area of the sample. D_2 is the distance between the center of the sample and center of the stilbene crystal of the detector. D_3 is the distance between the center of the target and the center of the stilbene crystal for the direct flux measurement, and D_4 the same distance for the scattered flux measurement. The average scattering angle is the angle between D_1 and D_2. All distances and angles in Table 2.2 are given in the laboratory coordinate system.

As can be seen in Table 2.2, two shadow cones were used, one of brass 10 in. long and one of tungsten 12 in. long.[9] Simple calculations show that tungsten is about 20 times better than brass for attenuating 18 MeV neutrons; a 10 in. long brass bar transmits only 0.7 percent of the neutron flux incident on it. The tungsten shadow cone was used in place of the brass shadow cone in order to decrease the contribution to the background caused by the neutron flux transmitted through the shadow cone. Actual measurements at 139° yielded a factor of two decrease in

---

[9]The tungsten bar stock was fabricated by the Fansteel Metallurgical Corporation of Chicago, Illinois and is sold under the trade name of Fansteel 77. Its composition is 89 percent tungsten, 7 percent nickel, and 4 percent copper; it is machinable with tungsten carbide cutting tools.

Table 2.2

SAMPLES, SHADOW CONES, AND GEOMETRICAL FACTS FOR THE DIFFERENTIAL CROSS SECTION EXPERIMENT

Average Scattering Angle (Degrees)	Month Data Taken	Shadow Cone Used	Sample Used	D_1 (cm)	D_2 (cm)	D_3 (cm)	D_4 (cm)
36	Feb. 1963	Tungsten	A	51.1	11.55	124.78	60.75
51	Oct. 1962	Brass	B	42.6	8.30	124.38	40.20
60	Feb. 1963	Tungsten	A	51.10	7.15	124.78	55.10
86	Oct. 1962	Brass	B	42.6	5.85	124.38	43.40
123.5	Feb. 1963	Tungsten	A	51.45	6.40	124.78	48.20
139	Feb. 1963	Tungsten	A	53.80	7.80	124.78	48.20

Annular Samples:

A: Sample cut from ATJ Graphite. 6 in. OD, 3 in. ID and 1.1 in. thick. Weight = 653.0 g.

B: Sample cut from Electrode Graphite. 6 in. OD, 3 in. ID and 1.1 in. thick. Weight = 651.3 g.

the statistical error between scattering ratio data taken with the brass shadow cone and the same data taken with the tungsten shadow cone.

The experimental geometry used for the total cross section experiment is shown in Figure 2.9.[10] The sample was 3 in. long and one inch in diameter and was machined from ATJ reactor grade graphite. It was placed midway between the target and the detector, and it was just large enough completely mask the stilbene crystal from target neutrons. The background was measured by replacing the sample with a 10 in. long by 1.5 in. diameter brass bar.

---

[10] The geometry is similar to the one discussed by D. W. Miller, op. cit.

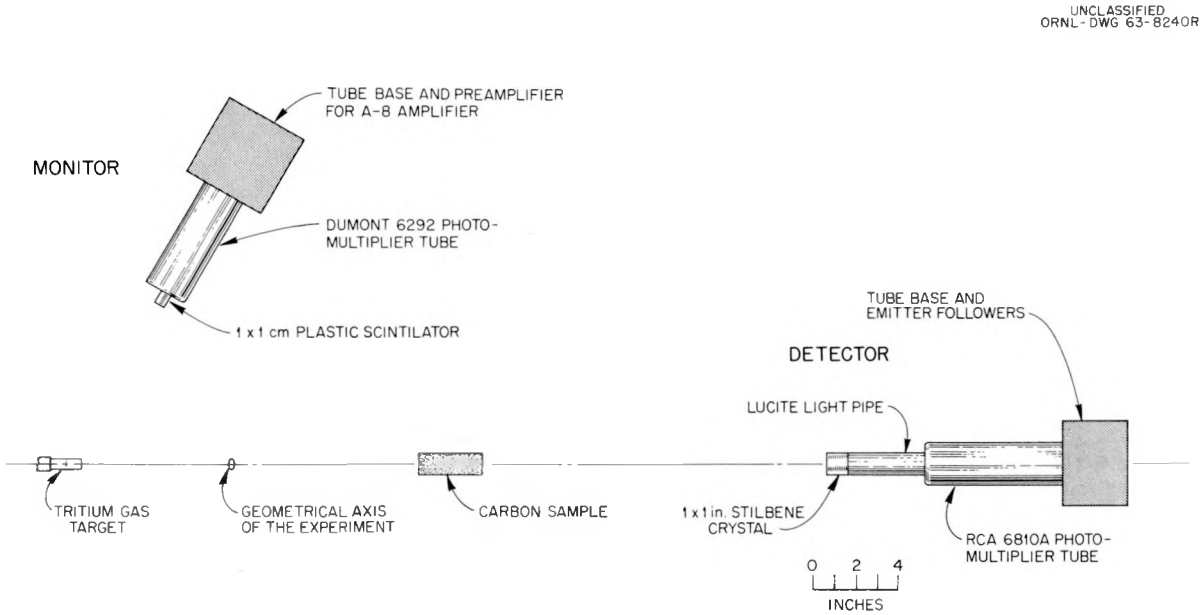

Figure 2.9. Schematic Diagram of the Geometry Used for the Total Cross Section Experiment. Cross-Sectional View Taken in a Horizontal Plane.

CHAPTER III

EXPERIMENTAL PROCEDURE

3.1 Introduction

This chapter deals with the determination of the energy of the neutrons emitted from the target, the calibration of the energy threshold (bias) of the detector in terms of neutron energy, and the experimental procedures used in both the differential cross section and total cross section experiments. Each of these three subjects are discussed in a general way. Representative samples of experimental data are given to illustrate various points made in the discussions.

3.2 The Determination of the Energy of the Neutrons Emitted from the Target

In order to determine the energy of the neutrons emitted from the target, we must first know the average deuteron energy in the target. The average deuteron energy in the double foil gas target was the deuteron energy at a point located on the geometrical axis (defined in Section 2.6) of the tritium gas cell midway between the foil window and the end of the cell. This average energy was calculated from the known energy of the deuteron beam prior to entering the target and from the calculated energy loss in the nickel foils and the helium and tritium gases.

The results of the calculation of the average deuteron energy in the gas target and the determination of the energy of the neutrons emitted from the target for a given set of target parameters are shown in Table 3.1a. The first column is the energy of the deuteron beam at

Table 3.1a

DEUTERON ENERGY LOSS IN THE GAS TARGET AND THE ENERGY OF THE NEUTRONS FROM THE TARGET

Incident Deuteron Energy (MeV)	Deuteron Energy Loss (keV)				Neutron Energy (MeV)
	In First Nickel Foil	In Helium Cooling Gas	In Second Nickel Foil	In First Half of T Gas Cell	
2.0	289	14	320	54	17.28
3.0	229	10	240	32	18.92
4.0	195	8	200	24	20.29
5.0	169	6	174	20	21.55

Target Parameters Used For Tables 3.1a, 3.1b, and 3.1c: 0.43 atm of T in 3 cm long Cell; 0.37 atm of He in 0.7 cm long cooling cell; and 0.1 mil thick nickel windows.

the entrance of the target. The energy loss in the nickel foils, in the helium gas, and in the tritium gas were obtained from graphs of energy loss versus incident deuteron energy. These graphs were prepared for a particular set of target parameters, like those given in Table 3.1a, from a set of dE/dx versus E curves.[1] Listed in the last column of Table 3.1a are neutron energies at zero degrees which were obtained from a table of neutron energy versus deuteron energy.[2]

The estimated energy spread in the neutron energy incident on the sample is given in Tables 3.1b and 3.1c for the differential cross section and the total cross section experiments. We define this energy spread, ΔE_5, by the formula

$$\Delta E_5 = \pm \sqrt{(\Delta E_2)^2 + (\Delta E_3)^2 + (\Delta E_4)^2} \quad , \tag{3.1}$$

where we have neglected the spread in the neutron energy resulting from the energy regulation system of the accelerator; this latter energy spread was approximately 1 to 3 keV. ΔE_2 was the energy spread introduced by the straggling of the deuteron beam in the two nickel foils as was calculated from formulae given in the literature.[3] It had a value of ± 22 keV for all deuteron energies between 2 and 5 MeV. ΔE_3 was neutron energy spread due to the half-thickness of the tritium gas

---

[1] W. Whaling, Handbuck der Physik, Vol. 34, ed. E. Flugge, (Berlin: Springer-Verlag, 1958), p. 193

[2] L. Blumberg and S. I. Schlesinger, Relativistic Tables of Energy Angle Relationships for the $T(p,n)He^3$, $D(d,n)He^3$, $T(d,n)He^4$ Reactions, A.E.C.U. 3118, (Washington: U. S. Government Printing Office, 1956), p. 191ff

[3] P. Marmier, Kernphysik, Part I, (Zurich: Verlag des Vereins der Mathematiker und Physiker an der ETH Zurich, 1960), p. 57

Table 3.1b

THE UNCERTAINTY IN THE ENERGY OF THE NEUTRONS FROM THE TARGET FOR THE DIFFERENTIAL CROSS SECTION EXPERIMENT

Incident Deuteron Energy (MeV)	Neutron Energy Spread Due to Half-thickness of the Tritium Target ΔE_3 (keV)	Neutron Energy Spread Due to Half-angular spread of the sample ΔE_4 (keV)	Energy Spread ΔE_5 (keV)	Uncertainty in the Foil Thickness and dE/dx ΔE_6 (keV)	Uncertainty in the Neutron Energy ΔE_7 (keV)
2.0	71	18	77	45	56
3.0	42	32	57	34	45
4.0	32	37	54	29	41
5.0	26	45	57	25	38

Table 3.1c

THE UNCERTAINTY IN THE ENERGY OF THE NEUTRONS FROM THE TARGET

FOR THE TOTAL CROSS SECTION EXPERIMENT

Incident Deuteron Energy	Neutron Energy Spread Due to Half-thickness of the Tritium Target ΔE_3 (keV)	Due to Half-angular spread of the sample ΔE_4 (keV)	Energy Spread ΔE_5 (keV)	Uncertainty in the Foil Thickness and dE/dx ΔE_6 (keV)	Neutron Energy ΔE_7 (keV)
2.0	71	5	75	45	56
3.0	42	5	48	34	43
4.0	32	5	39	29	39
5.0	26	5	34	25	35

target. ΔE_4 was the neutron energy spread due to the half-angular spread of the sample with respect to the target. It was obtained from tabulated values of neutron energy versus angle.[4] The uncertainty in the direction of the deuteron beam caused by straggling in the two nickel foils was approximately ± 0.7° and was neglected in the calculation of ΔE_4.[5] In the differential cross section experiment, the half-angular spread of the sample was approximately ± 2.5° about an average angle of 7.5°. ΔE_4 ranged between ± 18 and ± 45 keV for this experiment. In the total cross section experiment, the half-angular spread of the sample was ± 1.5° about zero degrees; hence, ΔE_4 was about ± 5 keV at all deuteron energies between 2 and 5 MeV.

The uncertainty (or standard deviation) in the neutron energy, ΔE_7, given in the sixth column of Tables 3.1b and 3.1c, was calculated from the equation

$$\Delta E_7 = \pm \sqrt{(\Delta E_2)^2 + a^2 [(\Delta E_3)^2 + (\Delta E_4)^2] + (\Delta E_6)^2} \; . \qquad (3.2)$$

It was necessary to know the uncertainty in the neutron energy because it entered into the calculation of the absolute error in the differential cross section (see Chapter IV), and into the determination of the uncertainty in the energy of the resonance found in the excitation curves. ΔE_2 has already been discussed. The uncertainty in the energy due to the energy spread introduced by the tritium cell, ΔE_3, and the finite angular spread of the sample, ΔE_4, is certainly less than either of these

---

[4] L. Blumberg and S. I. Schlesinger, op. cit.

[5] P. Marmier, op. cit.

two errors. This lowering of the uncertainty is taken care of by the factor a in equation (3.2). Although it is not clear as to what value should be taken for a, 1/3 is believed to be a reasonable estimate. ΔE_6 was the uncertainty in the neutron energy due to the uncertainty in the foil thickness and to the uncertainty in the value of dE/dx used to calculate the energy loss in the nickel foils. A ± 7 percent uncertainty in the foil thickness, and a ± 5 percent uncertainty in dE/dx were used in the calculation of ΔE_6. The ± 7 percent uncertainty was obtained from experimentally measured foil thicknesses of 13 sets of foils from the same batch of foils used in our experiment.[6]

3.3 The Calibration and Setting of the Energy Threshold or Bias of the Detector

The main function of the energy threshold of the detector, often called the detector bias, was to prevent inelastically scattered neutrons from the sample and neutrons produced by the $D(d,n)He^3$ reaction at the target and collimators from being recorded by the detector.[7] The detector bias was determined by the setting of the integral discriminator of the A-8 amplifier of the detector electronics (shown in Figure 2.1). A multichannel pulse height analyzer and the direct neutron beam were used to calibrate the bias setting in terms of neutron energy. This calibration was accomplished by taking spectra of monoenergetic neutrons

---

[6] We wish to thank Dr. R. W. Lamphere for giving us the data on these 13 sets of foils.

[7] Neutrons from the $D(d,n)He^3$ reactions will be referred to in the rest of this dissertation as d,d neutrons.

at a number of neutron energies between 12.8 and 21 MeV and by setting the discriminator at a new setting before each spectrum was taken.

One of these spectra is shown in Figure 2.3. A typical curve of discriminator setting versus channel number, which was obtained from a number of spectra like the one of Figure 2.3, is shown in Figure 3.1. The curve of neutron energy versus channel number obtained from the same set of spectra is shown in Figure 3.2. The energy calibration of the discriminator was carried out at least once a day as data were taken on the Van de Graaff accelerator.

In both the differential and the total cross section experiments, the detector bias was set at a neutron energy between the energy of the elastically scattered neutrons and the energy of neutrons inelastically scattered from the 4.4 MeV state of C^{12}. Within this restriction, the bias setting was set as low as possible so that a maximum sensitivity of the detector to elastically scattered neutrons was obtained. Representative values of these energies are tabulated in Table 3.2 for the scattering angles of 36 and 139 degrees. Formulae given in the literature were used in the calculation of these elastic and inelastic scattered neutron energies.[8]

The requirement on the bias energy that it be set so as to prevent the detector from recording d,d neutrons was automatically met when the bias energy was above the energy of the inelastically scattered neutrons. This was the case because the bias energy was always greater than 8 MeV,

---

[8] J. B. Marion, ed., 1960 Nuclear Data Tables, Part 3, (Washington: U. S. Government Printing Office, 1960), pp. 162-163

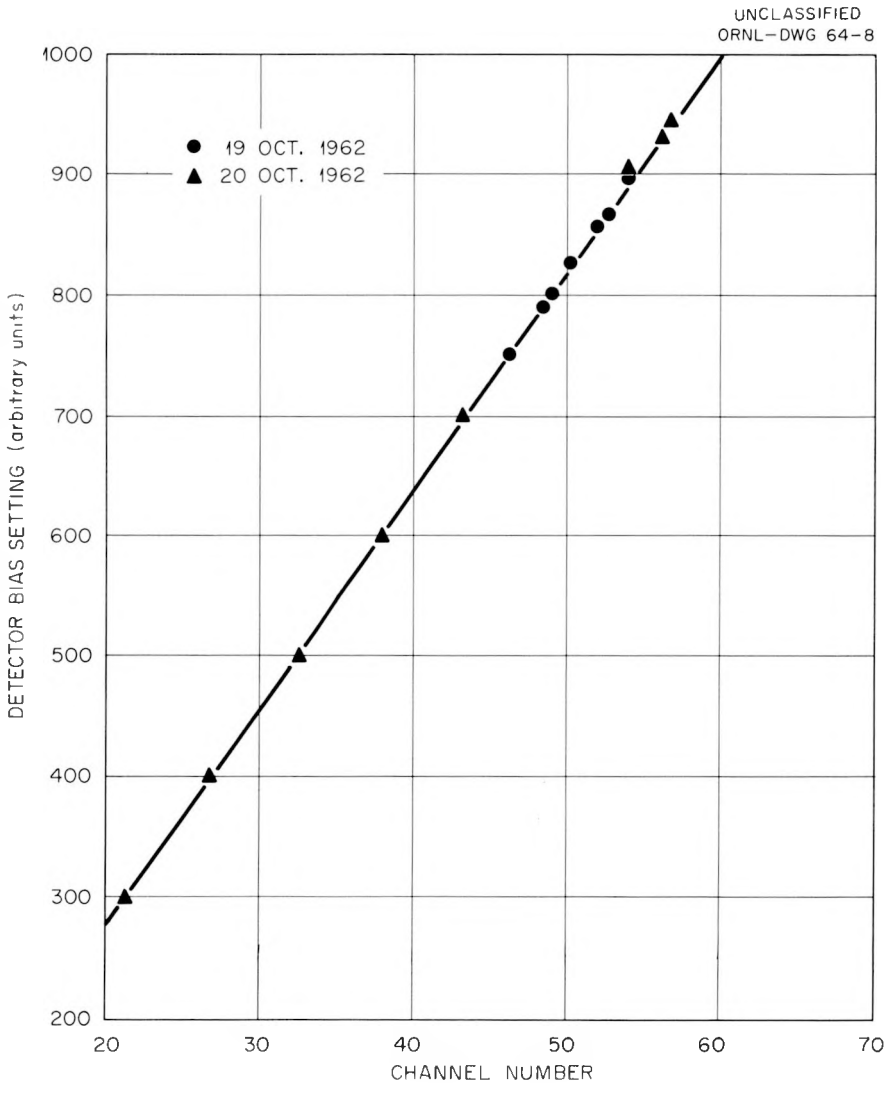

Figure 3.1. Detector Bias Calibration Curve.

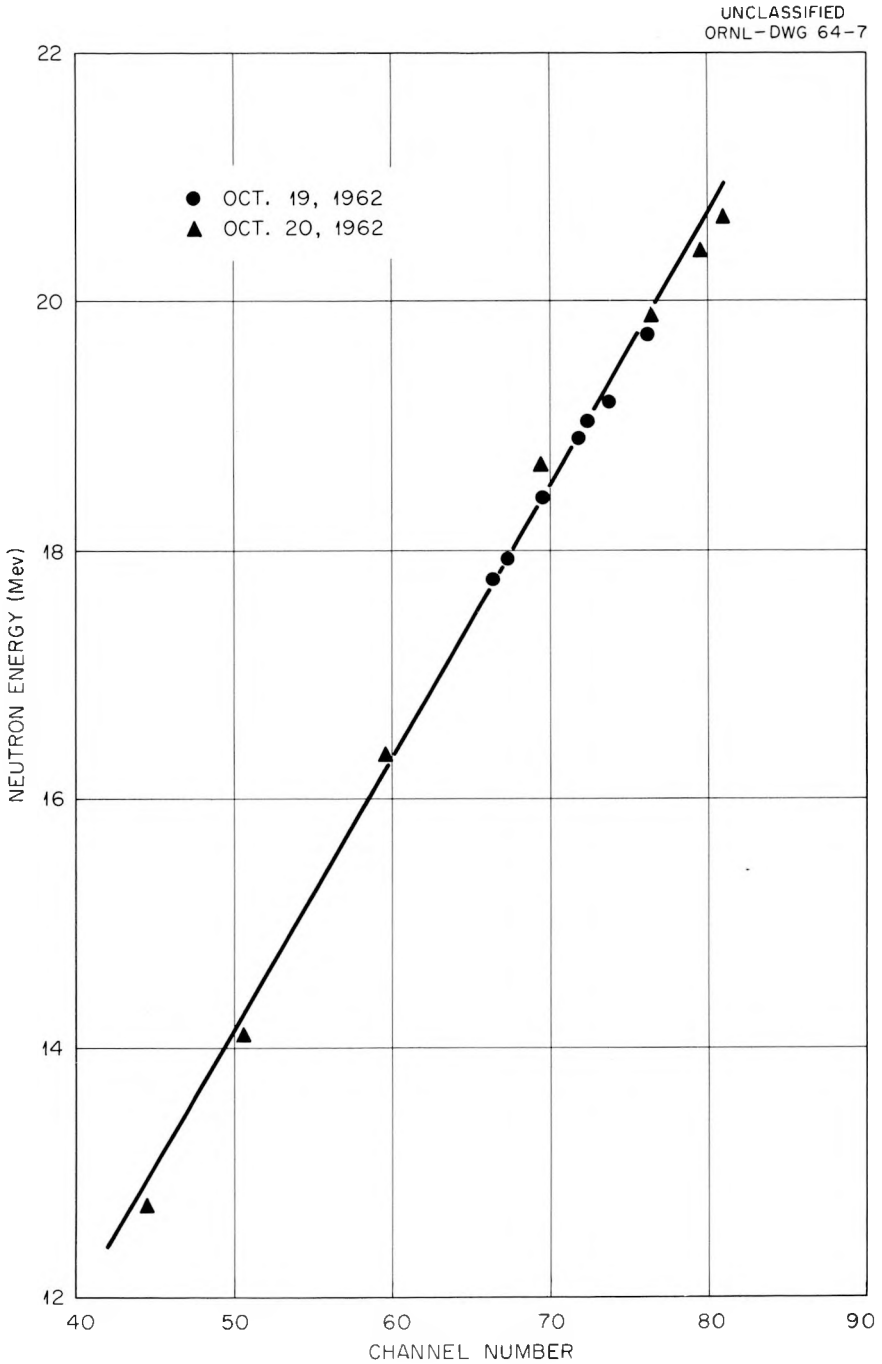

Figure 3.2. Detector Energy Calibration Curve.

Table 3.2

A SAMPLE OF VALUES OF DIRECT ENERGY, ELASTIC AND INELASTIC ENERGY, BIAS ENERGY, AND BIAS CONSTANT B(θ) USED IN THE DIFFERENTIAL CROSS SECTION EXPERIMENT FOR THE FIXED SCATTERING ANGLES OF 36° and 139°

Scattering Angle = 36°

Direct E	Elast E	Bias E	Inel E	B(36)
18.33	17.76	15.15	13.37	.83
18.47	17.89	15.29	13.50	.83
18.77	18.18	15.60	13.79	.83
19.06	18.46	15.89	14.07	.83
19.21	18.61	16.04	14.22	.84
19.48	18.87	16.30	14.48	.84
19.75	19.13	16.57	14.74	.84
20.02	19.39	16.82	15.01	.84
20.15	19.52	16.95	15.13	.84
20.42	19.78	17.23	15.39	.84
20.54	19.90	17.34	15.51	.84
20.68	20.03	17.32	15.65	.84

Scattering Angle = 139°

Direct E	Elast E	Bias E	Inel E	B(139)
17.48	13.04	10.77	9.22	.62
17.83	13.30	11.01	9.48	.62
18.16	13.55	11.22	9.73	.62
18.47	13.78	11.42	9.96	.62
18.77	14.00	11.64	10.18	.62
19.06	14.22	11.84	10.40	.62
19.21	14.33	11.92	10.51	.62
19.48	14.53	12.12	10.71	.62
19.75	14.74	12.32	10.91	.62
20.02	14.94	12.48	11.12	.62
20.29	15.14	12.68	11.32	.62
20.42	15.24	12.58	11.41	.62

and a 5 MeV deuteron produces a 8.2 MeV neutron from the $D(d,n)He^3$ reaction. The $D(d,n)He^3$ reaction occurred when the deuterons in the beam collided with deuterons which had been driven into the collimators of the target and into the end wall of the tritium gas cell.

In the differential cross section experiment, we also required that the detector bias be proportional to the incident neutron energy E_o. That is,

$$E_B = B(\theta_o)E_o \ , \tag{3.3}$$

where E_B is the detector bias energy, and $B(\theta_o)$ is the constant of proportionality. Representative values of $B(\theta_o)$ are given in Table 3.2. It is shown in Section 4.3 that when the detector bias is proportional to the direct neutron energy, the measured scattering ratio (defined in Chapter I) is approximately proportional to the differential cross section per steradian. Consequently, the scattering ratio would reflect any change in the differential cross section as a function of neutron energy.

3.4 The Experimental Procedure Used for the Differential Cross Section Experiment

The double foil gas target was installed in the target room on a beam port, and it was evacuated and very thoroughly checked for vacuum and pressure leaks.[9] During the time that the gas target was being set

---

[9] Suitable precautions were taken to minimize the local and the building-wide contamination that would have resulted from any serious accident involving the tritium gas from the target. Fortunately, no such accident occurred during our turns on the accelerator and only a small amount of local tritium contamination was experienced. This local contamination resulted primarily from the contact of pieces of experimental apparatus and hand tools with the target system.

up, the various components of the detector and the monitor electronic systems were put in their respective places in the target room and in the counting room. These components had been assembled and wired together beforehand so that the installation of them was straightforward and quickly done. The operation of the two electronic systems was checked by using neutrons from a Pu-Be neutron source.

Once a well regulated, steady deuteron beam from the accelerator had been obtained, the gas target was aligned so that the beam passed through the two collimating apertures of the target, through the helium cooling cell, and into the tritium gas cell. This alignment was achieved by moving the target about so that the beam current measured on the gas cell was maximized, and the beam currents measured on the first and second collimators of the target were minimized. When the optimum position was reached, the target was locked into position. After the alignment of the target had been completed, the analyzing magnet of the accelerator was calibrated, if this was necessary, using the reaction $T(p,n)He^3$ and a zirconium tritide target.

The apparatus and the support platform were then aligned using the position of the gas target to define the geometrical axis of the experiment. The ring geometry for a fixed scattering angle was set up, and the various geometrical distances were recorded. Care was taken to align the apparatus to the nearest 1/32 inch. The stops that were employed to mark the positions of the sample and the detector on the support platform were secured rigidly to the platform. These stops permitted the positions of the sample and the detector to be reproducible to within about 1/32 inch. The support member for the shadow cone was designed so that the

shadow cone could be removed from the support platform and replaced again in a position that was within at least 1/32 inch of its original position. The monitor detector was mounted on a rigid stand and placed at an angle of about 55° with respect to the geometrical axis of the experiment and at a distance of 9 inches from the center of the tritium gas cell.

The next step in the procedure was to find a hole-free set of nickel foils for the target. The search for a good set of foils had to be made using the gas target system because the foils were so fragile that they could be handled, without damage, only the single time that it took to install them in the foil receptacles of the helium cooling cell of the target. After installing a set of nickel foils in the target, the tritium gas cell, the helium cell, and the section of beam tube located in front of the helium cell were evacuated and isolated from each other by turning off valves on the gas distribution manifold. The helium cell was then brought up to atmospheric pressure. If the pressure changes in the tritium cell or in the section of beam tube were negligible after a ten minute wait, the foils were considered to be free of holes. If the pressure at either position changed, the corresponding foil was removed and replaced with a new one and the checking procedure was repeated. It took about 30 minutes to an hour to carry out one complete cycle in the checking procedure. This procedure often had to be repeated a number of times before a hole-free set of foils was found. After a hole-free set of nickel foils had been found, the target was evacuated and filled with tritium gas; the helium cooling gas was then turned on.

The next step in the experimental procedure was to adjust and to calibrate the electronics. The pulse shape discrimination circuit of the detector was adjusted so that an optimum separation was obtained between neutron pulses and gamma ray pulses. The adjustment of the circuit was monitored with the display oscilloscope. Figure 3.3 shows the display which corresponds to an optimum adjustment of the circuit. The bias or integral discriminator setting on the A-1D amplifier shown in Figure 2.1 was set at a pulse height midway between the average neutron slow-component pulse height and the average height of the slow-component gamma ray pulse height. This setting is illustrated in Figure 3.3. With the bias of the A-1D amplifier set at this level, the detector would record only neutrons having an energy equal to or greater than the energy threshold or bias of the detector.

After these operations, the detector was calibrated in terms of neutron energy (see Section 3.3). For this calibration, the sample and the shadow cone were removed from the support platform, and the detector was exposed to a direct beam of neutrons produced by a deuteron beam on the target of 0.1 μa. The deuteron beam current was purposely made small to prevent pulse pile-up in the detector. The detector was rotated about the target in a horizontal plane to different platform rotation angles to obtain the range of neutron energies needed for the calibration (see Figure 3.4). With the completion of the calibration of the detector bias, a table of values of bias settings versus neutron energy was constructed for a fixed value of $B(\theta)$. During the collection of data, the detector bias was set at a value E_B given by Eq. 3.3. The adjustment of the monitor system on the multichannel analyzer and setting the integral

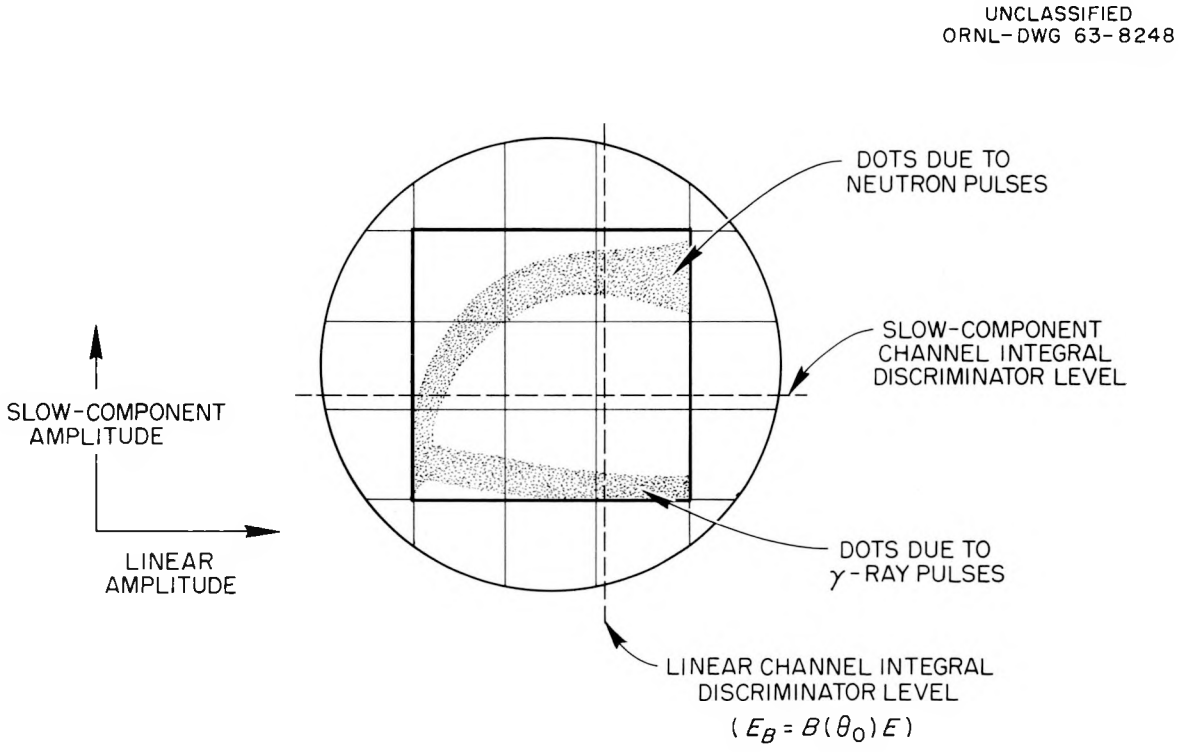

Figure 3.3. A Sketch of the Oscilloscope Display (Display Gate Triggered by Every Detected Particle).

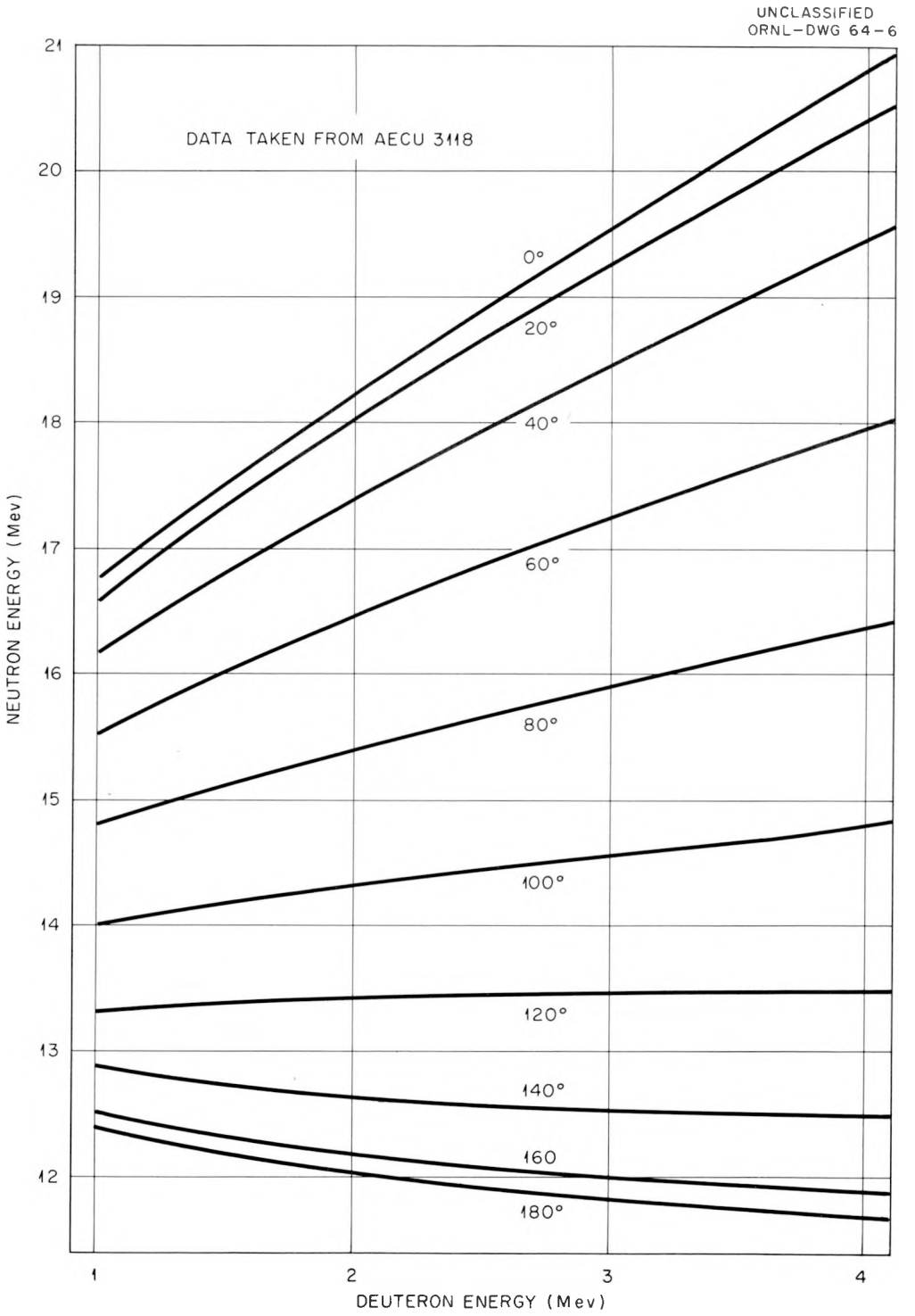

Figure 3.4. Energy of Neutrons from the $T(d,n)He^4$ Reaction as a Function of the Deuteron Energy and the Angle of Observation.

discriminator of the amplifier at a pulse height above the maximum pulse height corresponding to gamma rays and/or d,d neutrons.

The procedure for taking the data consisted of an orderly set of operations by which the scattered neutron flux, the background neutron flux, and the direct neutron flux were measured. The three flux measurements, which were made at a given neutron energy, were carried out one right after the other and as quickly as possible in order to minimize effects upon the data caused by any slow drifts in the electronics and in the energy calibrations. The procedure for the flux measurements were as follows:

1) The energy of the neutrons emitted from the target was fixed at a particular value by a well defined deuteron beam energy. The detector bias was set at a value which corresponded to the value of the incident neutron energy.

2) The sample, shadow cone, and the detector were placed in the proper position for the scattered flux measurement. A measurement of the scattered neutron flux was carried out for a preset number of monitor counts adequate to give the desired counting statistics.

3) The sample was removed. The background neutron flux was measured for a preset number of monitor counts adequate to give the desired counting statistics.

4) The shadow cone was removed, and the detector was moved back about 124 cm from the center of the gas target. The direct neutron flux was measured for a preset number of monitor counts adequate to give the desired counting statistics.

The deuteron beam current on the gas target was kept as constant as possible during the three flux measurements. The flux measurements were repeated at neutron energy intervals of approximately 150 keV between 17.2 and 21 MeV. Measurements at some of the energies were repeated. The repeated measurements agreed within counting statistics. It took anywhere from 20 minutes to one hour to complete the measurements at one energy and to change the neutron energy to the next value.

A scattering ratio R, which is defined in Chapter I, and the approximate statistical error in R were calculated at each neutron energy immediately after the flux measurements at an energy were completed. Equations for R and the statistical error in R in terms of the detector and the monitor counts are given in Appendix A. When the 51 and 85 degree data were taken, a number of background measurements at some of the energies were skipped because experience had shown that they could be obtained by interpolation from measured background values. Extrapolated values of the background were used in the calculation of the scattering ratio for these energies. As the data were taken and R calculated, a graph of R versus the direct neutron energy was plotted (see Figure 4.5). Since R was approximately proportional to the differential cross section, the graph illustrated the change in the relative differential cross section with energy. It, therefore, served as a guide in the choice of neutron energies at which data could be taken to best describe the resonance effects that were observed. The graph also served to point up, immediately, equipment failures, misalignment and errors made in the procedures. Thus, not much time was lost in the experiment taking worthless data that otherwise might have been thought to be correct.

3.5 Measurement of the Total Cross Section

Essentially the same experimental apparatus and experimental procedures were used in the total cross section experiment as were used in the differential cross section experiment. The sample and the shadow cone used in the differential cross section experiment were simply removed. The sample for the total cross section experiment was substituted in their place, and distances and alignments were changed. The detector bias was set so that it was necessary to change it only once for about every 1 MeV change in the neutron energy. When set in this manner the bias energy was high enough so that inelastically scattered neutrons were not recorded.

The alignment of the sample, target, and the detector was done with an aligning bar which exactly replaced the sample in the sample holder and which had center points at either end which defined the axis of the bar. This axis was positioned by changing the position of the sample holder until the axis of the bar and the geometrical axis of the experiment were identical. The bar spaced the sample holder, hence the sample, to a position midway between the detector and the target. When the target, the sample, and the detector were properly aligned, the sample completely masked the detector from the direct flux of neutrons from the target. The alignment was checked periodically as data were taken.

The procedures for taking data were essentially those followed in the differential cross section experiment. The sample was put in the sample holder, and an attenuated flux was measured. The sample was removed, and a direct flux was measured. An attenuated bar was put in the sample holder, and the background flux was measured. For these three

measurements the position of the detector remained the same, and the beam current was kept as constant as possible. Measurements were taken at approximately 150 keV intervals between 17.5 and 21 MeV. A large number of the measurements were repeated. The total cross sections calculated from these repeated measurements agreed within counting statistics. It took an average of about 30 minutes to take the data at one energy and to change the neutron energy to the next value.

The transmission, which is defined in Chapter I, and the statistical error in the transmission were calculated at each energy as the data were taken. Extrapolated values of the background were used in the calculation of the transmission at those energies at which no background was taken. The total cross section was calculated from the transmission using equation (5.4) and plotted as a function of neutron energy. The graph was similar to the graph illustrated in Figure 5.2. It was used to monitor the progress of the experiment.

CHAPTER IV

THE DIFFERENTIAL CROSS SECTION EXPERIMENT

4.1 Introduction

An equation for the differential cross section at an average scattering angle is derived and then evaluated by numerical integration. This equation contains corrections for the finite size of the sample, for the finite size of the detector, for absorption in the sample, and for the angular spread of the sample with respect to the detector. These corrections were appreciable in the present experiment, and therefore had to be considered. A correction factor for multiple scattering in the sample and a correction factor for the polarization of the neutrons from the target are derived and calculated. The final results, which were obtained after all corrections had been made, are presented along with the errors in these results. The physical significance of these results is dealt with in Chapter VI.

4.2 The Definition of Symbols and Coordinate Systems

$I(\phi,E_\phi)$ = number of neutrons of energy E_ϕ per steradian per sec emitted from the target at an angle ϕ.

$\sigma_R(\phi,E_\phi)$ = differential reaction cross section for the $T(d,n)He^4$ reaction for neutrons emitted from the target at an angle ϕ with an energy E_ϕ.[1]

---

[1] In the calculations which follow, this cross section was obtained from N. Jarmie and J. D. Seagrave, eds., Charge Particle Cross Sections, LA-2014, (Washington: U. S. Government Printing Office, 1957), p. 42.

n_1 = number of C^{12} nuclei per cm^3.

n_2 = number of hydrogen nuclei per cm^3 in the stilbene crystal.

V_2 = volume of the stilbene crystal.

$\epsilon(E_i, E_B)$ = fraction of the proton recoil spectrum counted by the detector for neutrons of energy E_i incident on the stilbene crystal and for a detector bias energy of E_B. It can be shown that

$$\epsilon(E_i, E_B) = \frac{E_i - E_B}{E_i} \quad ,$$

where end effects, absorption, and multiple scattering in the crystal have been neglected.

$\sigma_{np}(E_i)$ = neutron-proton total cross section for neutrons of energy E_i.[2]

$\sigma_T(E_i)$ = total neutron cross section for C^{12} for neutrons of energy E_i.[3]

$\sigma(\theta)$ = differential elastic cross section for neutrons of incident energy E_i elastically scattered from C^{12} into a scattering angle of θ.

$E_{el}(\theta)$ = the energy of neutrons elastically scattered from C^{12} into an angle θ.

E_o = the energy of neutrons emitted from the target at 0°.

---

[2] In the calculations which follow, this cross section was obtained from J. B. Marion, op. cit., p. 111.

[3] Measured total cross sections were used in the calculations.

$k(\theta)$ = fraction of the incident energy carried away by a neutron elastically scattered from C^{12} into a scattering angle of θ; i.e., $E_{el}(\theta) = k(\theta)E_{\phi}$.

θ = $\cos^{-1}(\vec{k}_1 \cdot \vec{k}_2)$, where $\vec{k}_1$ and $\vec{k}_2$ are unit vectors defined implicitly in Figure 4.1.

R = scattering ratio at an average scattering angle θ_o. R is the ratio of the scattered neutron intensity divided by the direct neutron intensity where both scattered and direct intensities have been corrected for background; see Appendix A.

The other quantities used in the following derivations are defined in the text or implicitly in Figures 4.1, 4.2, 4.4, or 4.6.

The derivation of the equation used to calculate the differential cross section involves integrations over the sample volume and the volume of the stilbene crystal. For this reason, two separate coordinate systems must be defined. Cylindrical symmetry of the sample and of the stilbene crystal with respect to the geometrical axis, and the fact that the front face planes of the sample and the stilbene crystal are parallel to each other and are both perpendicular to the geometrical axis make cylindrical polar coordinates an ideal choice for the two coordinate systems. The two coordinate systems are illustrated in Figures 4.1 and 4.2. The origin of the sample coordinate system is at the point of intersection of the front face plane of the sample and the geometrical axis, and the origin of the crystal coordinated system is at the intersection of the front face plane of the stilbene crystal and the geometrical axis. Positive x direction is chosen to be the right of the origins along the geometrical

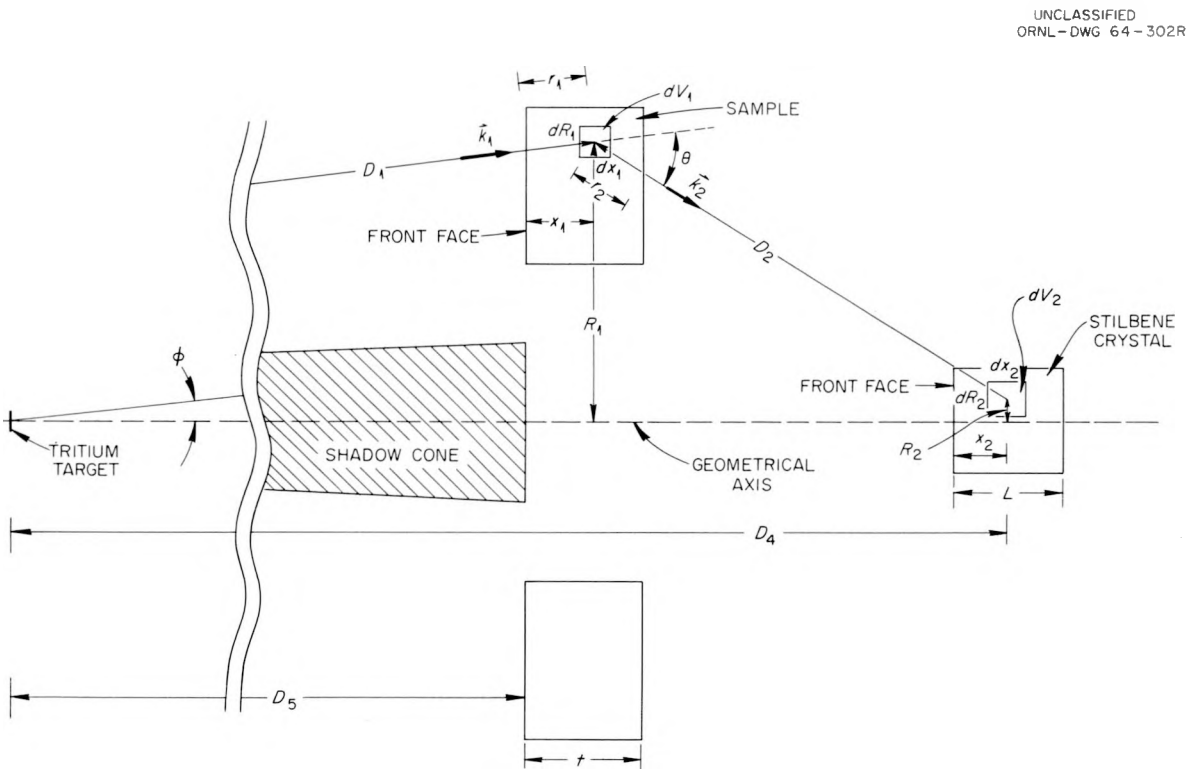

Figure 4.1. A Cross-Sectional View of the Geometry Used for the Measurement of the Differential Cross Section for 36°.

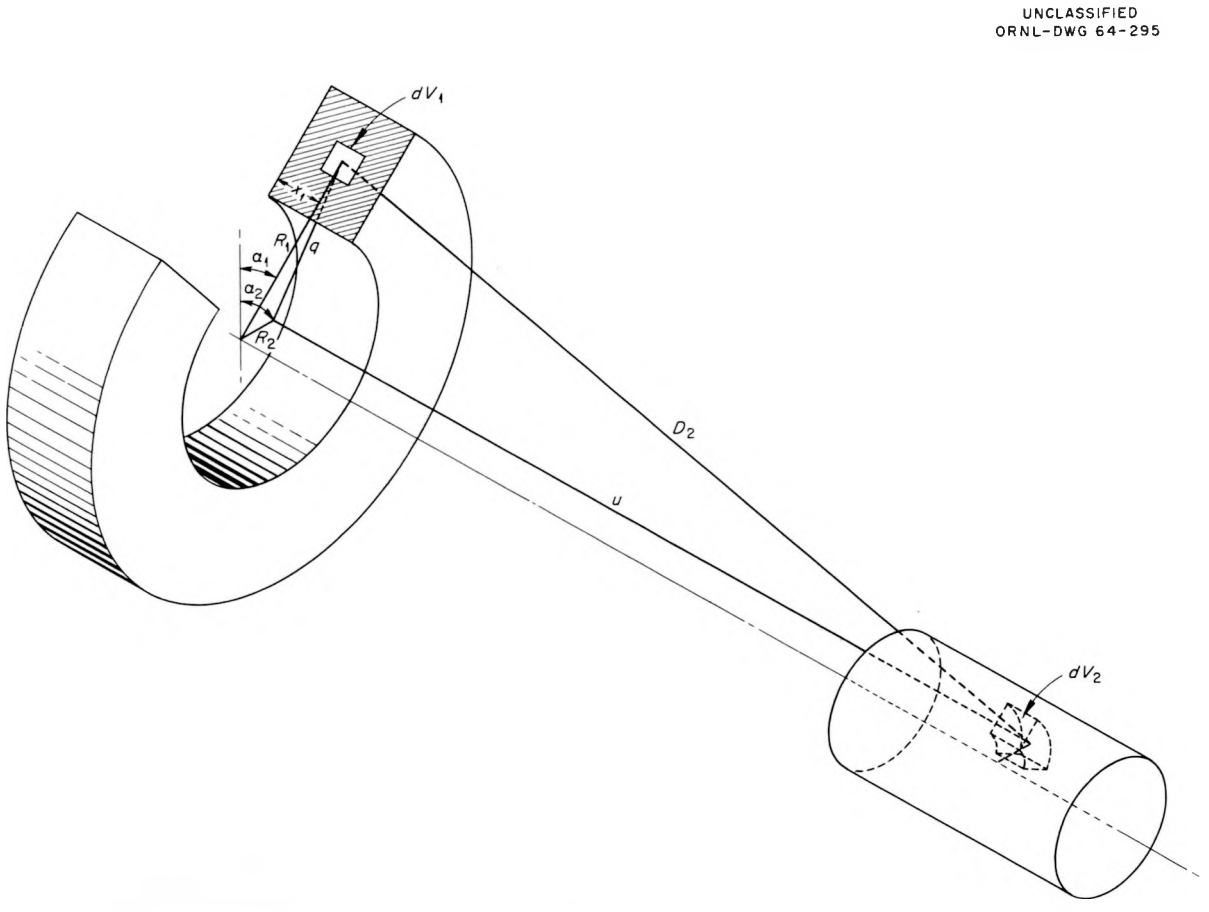

Figure 4.2. A Three Dimensional View of the Geometry.

axis of both of the coordinate systems. When the polar angles $\alpha_1 = 0$ and $\alpha_2 = 0$,

$$\frac{\vec{R}_1}{|\vec{R}_1|} = \frac{\vec{R}_2}{|\vec{R}_2|} \quad ;$$

that is, the plane of zero α_1 and α_2 is the plane of Figure 4.1. The symbolic volume elements of the sample and the stilbene crystal coordinate systems are

$$dV_1 = R_1 \, dR_1 \, d\alpha_1 \, dx_1,$$

and

$$dV_2 = R_2 \, dR_2 \, d\alpha_2 \, dx_2,$$

respectively.

4.3 The Derivation and the Solution of the Equation Used to Calculate the Differential Cross Section

Since the geometry in the present experiment was such that the source of neutrons was essentially a point source, a point source will be assumed in the following derivation. We will also assume that only single scattering events occurred in the sample.

With these assumptions, we can write that the symbolic number of neutrons per second which are elastically scattered by the volume element dV_1 into an angle Θ and leave the sample is, to within several percent,

$$dF_1 = \left[I(\phi, E_\phi) \, \frac{R_1 \, dR_1 \, d\alpha_1}{0_1^2} \, e^{-\sigma_T(E_\phi) n_1 r_1} \right] e^{-\sigma_T(E_d) n_1 r_2} \, \sigma(\theta) \, n_1 \, dx_1, \tag{4.1}$$

where the factor in the brackets is the neutron intensity incident on dV_1, and $\exp[-n_1\sigma_T(E_{el})r_2]$ is the attenuation factor for scattered neutrons leaving the sample. Of these scattered neutrons, only dF_s are recorded by the detector. dF_s is given by

$$dF_s = \frac{\sigma_{np}(E_d)\ \epsilon(E_d, E_\theta)\ n_2}{D_2^2}\ dF_1\ dV_3,$$

where we define dV_3 as a symbolic volume element of a spherical polar coordinate system which has its origin at the center of dV_1. dV_3 lies in the stilbene crystal at a distance D from the origin of this spherical polar coordinate system. Such an equation as the one above would be extremely difficult to integrate in its present form. In order to make it more manageable, we replace dV_3 by dV_2, the volume element of the cylindrical polar coordinate system of the stilbene crystal. This simplification introduces a systematic error in the absolute value of the cross section which is roughly estimated to be of the order of about ± 10 percent. The simplified equation is

$$dF_s = \frac{\sigma_{np}(E_d)\ \epsilon(E_d, E_\theta)\ n_2}{D_2^2}\ dF_1\ dV_2. \tag{4.2}$$

The total rate of neutrons, F_s, recorded by the detector is obtained by replacing dF_1 in equation (4.2) by the right-hand side of equation (4.1) and integrating the resulting equation over the volume of the sample and the stilbene crystal giving

$$F_s = \int_{V_1}\int_{V_2} \frac{I(\phi, E_\phi)\, e^{-n_1[\sigma_T(E_\phi)r_1 + \sigma_T(E_d)r_2]}}{(D_1 \cdot D_2)^2}\ \sigma(\theta)\ n_1 n_2\ \sigma_{np}(E_d)\ \epsilon(E_d, E_\theta)\ dV_1\, dV_2. \tag{4.3}$$

When the detector is exposed to the direct neutron beam, the total neutron intensity recorded by the detector is

$$F_D = I(0,E_o)\frac{\pi R^2}{D_3^2}\sigma_{np}(E_o)n_2 L\epsilon(E_o,E_B). \tag{4.4}$$

Since the right-hand side of equation (4.4) is constant with respect to the variables of integration in equation (4.3), the integrand of equation (4.3) is simplified by dividing equation (4.3) by equation (4.4). The resulting equation is

$$R = H\int_{V_1}\int_{V_2} G\,\sigma(\theta)\,dV_1\,dV_2 \tag{4.5}$$

where

$$R = F_S/F_D,$$

$$H = \frac{I(\phi,E_\phi)}{I(0,E_o)}\cdot\frac{\sigma_{np}(E_{el})}{\sigma_{np}(E_o)} = \frac{\sigma_R(7.5,E_o)}{\sigma_R(0,E_o)}\cdot\frac{\sigma_{np}(E_{el})}{\sigma_{np}(E_o)}, \tag{4.6}$$

$$G = \frac{n_1}{V_2}\cdot\left(\frac{D_3}{D_1 D_2}\right)^2\cdot\frac{\epsilon(E_{el},E_B)}{\epsilon(E_o,E_B)}\cdot e^{-n_1\left[\sigma_T(E_o)r_1+\sigma_T(E_{el})r_2\right]}. \tag{4.7}$$

The substitution of E_o for E in equations (4.6) and (4.7) and the removal of H from the integral of equation (4.5) are discussed below.

Let us consider the factor

$$H = \frac{I(\phi,E_\phi)}{I(0,E_o)}\,\frac{\sigma_{np}(E_{el})}{\sigma_{np}(E_o)}.$$

Since the mean half angle $\bar{\phi}$ which the sample subtends with the geometrical axis at the target ranges between 6° and 7.5° for all geometries studied,

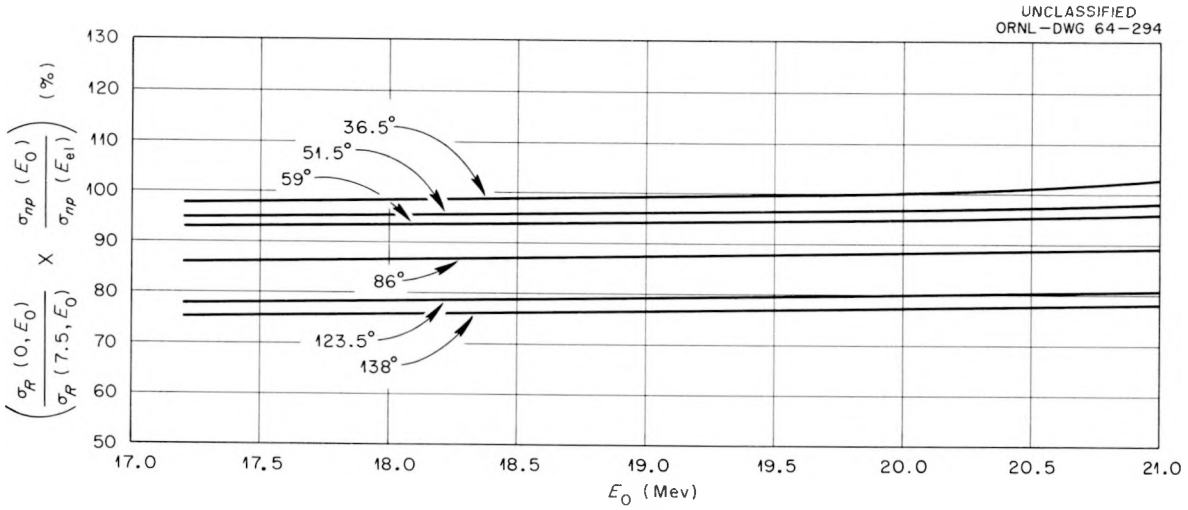

Figure 4.3. H^{-1} Versus Neutron Energy for Six Different Scattering Angles.

we can replace ϕ in the factor by $\tilde{\phi} = 7.5°$. As a consequence of the smallness of $\tilde{\phi}$, $E_o - E_\phi \simeq 0.1$ MeV; hence, to a good approximation

$$E_\phi \simeq E_o.$$

The ratio $I(\phi, E_\phi)/I(0, E_o)$ can be replaced by its equivalent, the ratio of the reaction cross sections: $\sigma_R(\phi, E_\phi)/\sigma_R(0, E_o)$. Incorporating these changes into the factor gives

$$H = \frac{\sigma_R(7.5, E_o)}{\sigma_R(0, E_o)} \cdot \frac{\sigma_{np}(E_d)}{\sigma_{np}(E_o)} .$$

The reciprocal of H is plotted in Figure 4.3. We note in the figure that, for a given mean scattering angle, there is very little percentage change in H as a function of neutron energy in the energy range of 17.2 to 21.0 MeV. We also note that, for a given energy, H changes only a few percent as the scattering angle is varied 10 degrees or so about any of the mean scattering angles. We conclude from this discussion that H can be considered constant with respect to the variables of integration in equation (4.5); and, can therefore be removed from the integral.

The approximate solution of equation (4.5) for the cross section $\sigma(\theta)$ is obtained by first expanding the cross section in a Taylor's series about the average scattering angle θ_o (defined implicitly in Figure 4.4) and neglecting third and higher order terms. This expansion is

$$\sigma(\theta) = \sigma(\theta_o) + (\theta - \theta_o)\sigma'(\theta_o) + 0.5(\theta - \theta_o)^2\sigma''(\theta_o) + \cdots, \tag{4.8}$$

where $\sigma'(\theta_o)$ and $\sigma''(\theta_o)$ are the first and second derivatives of $\sigma(\theta)$ with respect to θ. Next, equation (4.8) is then substituted into equation

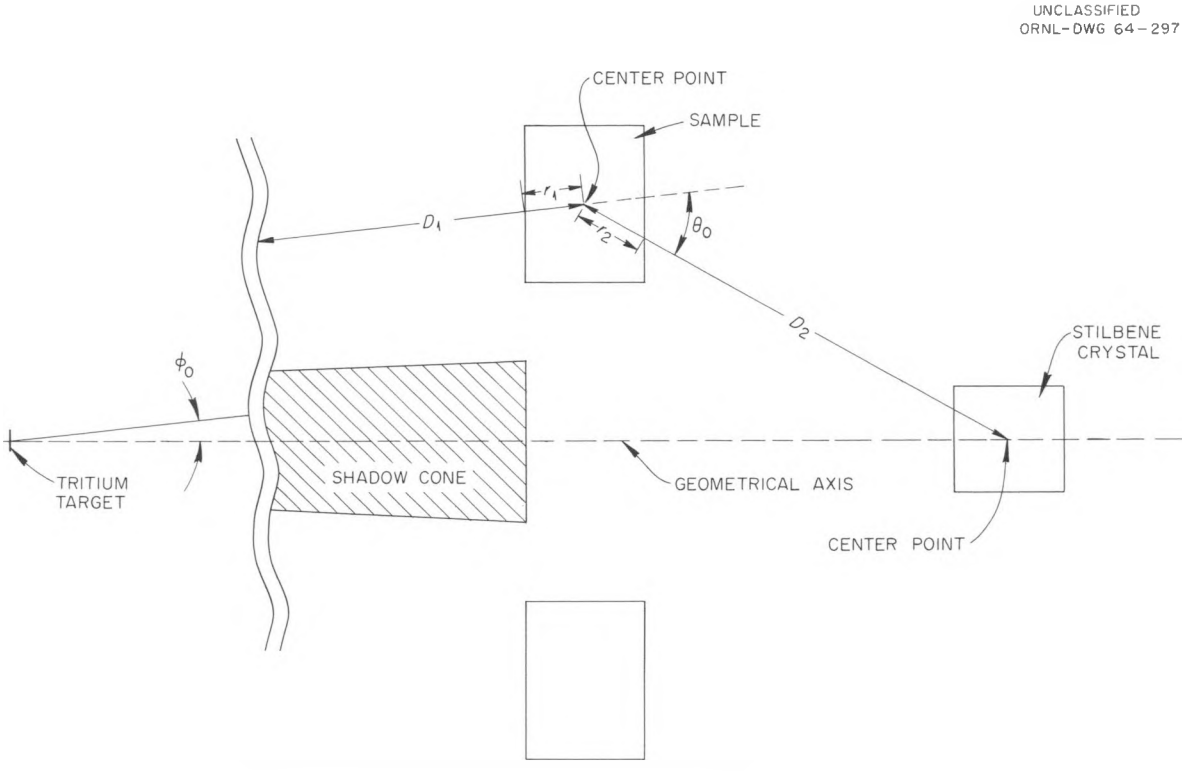

Figure 4.4. The Definition of the Average Scattering Angle for the 36° Geometry.

(4.5) to give the solution

$$\sigma(\theta_o) = \frac{R}{H\int_{V_2}\int_{V_1} G\,dV_1\,dV_2} - \frac{\int_{V_2}\int_{V_1} G\left[(\theta-\theta_o)\sigma'(\theta_o) + 0.5(\theta-\theta_o)^2\sigma''(\theta_o)\right]dV_1\,dV_2}{\int_{V_2}\int_{V_1} G\,dV_1\,dV_2}. \tag{4.9}$$

The first term of equation (4.9) is the calculated cross section corrected for absorption in the sample and for the finite size of the detector and of the sample. The absorption correction is accomplished by the factor

$$\exp\left[-n_1\left\{\sigma_T(E_o)r_1 + \sigma_T(E_d)r_2\right\}\right],$$

which is contained in G; and the integrals over the detector and sample volumes are the finite size corrections. The second term of equation (4.9) is the cross section which results from the angular spread of the sample with respect to the detector. This cross section is added to or subtracted from (depending upon the sign of the integral) the cross section calculated by the first term of the equation to correct it for the angular spread of the sample.

In the present experiment, we were primarily interested in the relative differential cross section as a function of neutron energy at a fixed scattering angle θ_o. Since the corrections for absorption, angular spread, and finite sample and detector size were either constant or slowly varying functions of neutron energy, we initially omitted all of these corrections and reduced equation (4.9) to

$$\sigma(\theta_o) = \frac{R}{NH}\cdot\frac{\epsilon(E_o, E_B)}{\epsilon(E_d, E_B)}\cdot\left[\frac{D_1\cdot D_2}{D_3}\right]^2. \tag{4.10}$$

Thus, we obtained an equation for calculating a relative differential cross section. In equation (4.10), $N = n_1 V_1$; and D_1 and D_2 are defined implicitly in Figure 4.4.

The calculation of the relative differential cross section was greatly facilitated during the experimental phase of the work by setting the detector bias, E_B, so that

$$E_B = B(\theta_o)E_o \ , \tag{4.11}$$

where $B(\theta_o)$ is a constant. Introducing this equation into equation (4.10) gives the equation

$$\sigma(\theta_o) = R\left\{\frac{k(\theta_o)\left[1 - B(\theta_o)\right]}{HN\left[k(\theta_o) - B(\theta_o)\right]}\left[\frac{D_1 D_2}{D_3}\right]^2\right\}. \tag{4.12}$$

Since the factor in the brackets is independent of neutron energy, $\sigma(\theta_o)$ is directly proportional to R and therefore has the same energy dependence as R. An example (for $\theta_o = 36°$) of a curve of R versus neutron energy is shown in Figure 4.5. Curves such as this one were plotted as data were taken so that the progress of the experiment could be continuously monitored.

In order to obtain the relative differential cross section to a better approximation, and in order to express it in absolute units, the cross section was calculated by equation (4.9). As was mentioned above, equation (4.9) contains corrections for absorption, angular spread, and finite sample and detector size. The general method used to evaluate equation (4.9) is best illustrated by evaluating a simpler equation which is obtained from equation (4.9) when the corrections for angular spread

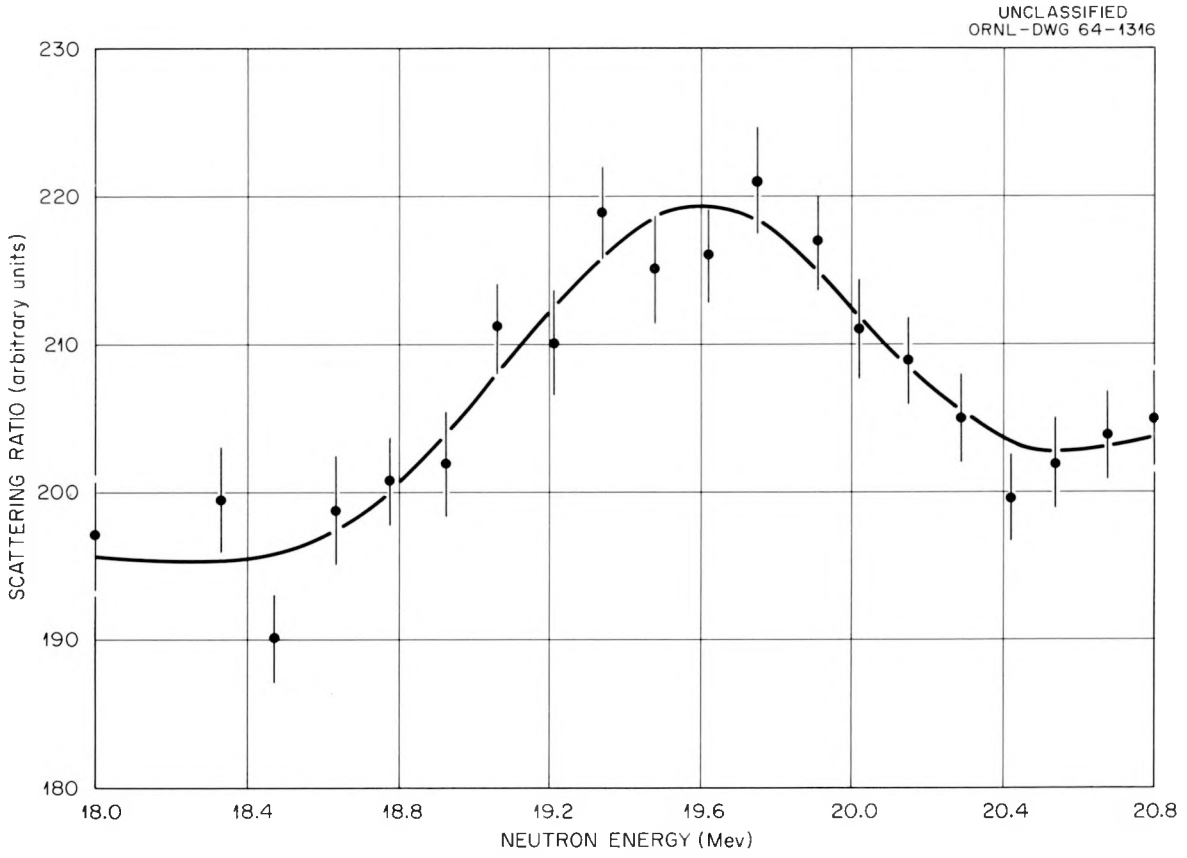

Figure 4.5. The Scattering Ratio for 36° as a Function of Neutron Energy.

and finite detector size are neglected. This equation is

$$\sigma(\theta_o) = \frac{R}{2\pi V_2 H \int_{x_1}\int_{R_1} G\, R_1\, dR_1\, dx_1} \quad . \tag{4.13}$$

After numerical integration, equation (4.13) reduces to

$$\sigma(\theta_o) = \frac{R^m \epsilon(E_o^m, E_B^m)}{H^m\, 2\pi n_1 D_3^2} \left[\sum_{\lambda=1}^{a} \sum_{j=1}^{b} \frac{\epsilon(E_{el}^{ijm}, E_B^m)}{(D_1^{ij} \cdot D_2^{ij})^2}\, e^{-n_1\left[\sigma_T(E_o^m) r_1^{ij} + \sigma_T(E_{el}^{ijm}) r_2^{ij}\right]}_{R_1^{ij}\ \Delta R_1 \Delta x_1} \right]^{-1} \tag{4.14}$$

where the energy dependence of the variables is indicated by the superscript m; and where, for the geometry of the present experiment,

$$\Delta R_1 = 3.81/a, \qquad \Delta x_1 = 2.79/b,$$

$$R_1^i = 3.81 + \Delta R(i - 0.5), \qquad x_1^j = \Delta x_1 (j - 0.5),$$

$$(D_1^{ij})^2 = (R_1^i)^2 + (D_3 + x_1^j)^2, \qquad (D_2^{ij})^2 = (R_1^i)^2 + (D_4 - D_3 - x_1^j)^2,$$

$$\epsilon(E_o^m, E_B^m) = \frac{E_o^m - E_B^m}{E_o^m}, \qquad \epsilon(E_{el}^{ijm}, E_B^m) = \frac{E_{el}^{ijm} - E_B^m}{E_{el}^{ijm}},$$

$$\theta^{ij} = \cos^{-1}\left\{ \frac{D_4^2 - (D_1^{ij})^2 - (D_2^{ij})^2}{2 D_1^{ij} D_2^{ij}} \right\},$$

$$E_{el}^{ijm} = 5.92 \times 10^{-3} E_o^m \left\{ \cos\theta^{ij} + \left[144 - \sin^2\theta^{ij}\right]^{1/2} \right\}^2,$$

$$r^{ij} = 1.01 x_1^j \quad . \qquad \text{equations (4.15)}$$

Measured values of r_2^{ij} were used in the calculations. Some of the geometrical quantities in equations (4.15) are illustrated in Figure 4.6 for the case of summation limits a = b = 2. The actual numerical calculation of the cross section by equation (4.14) (and also by equation (4.16)) was carried out on a CDC 1604A digital computer.

The cross section was calculated by equation (4.14) at each value of neutron energy E_o^m and at each average scattering angle θ_o. R was calculated by equations given in Appendix A. H was taken from Figure 4.3. E_B^m was calculated at each E_o^m by formulae obtained by least squares fitting straight lines to the measured energy and bias calibration data; see Figures 3.1 and 3.2 for a sample of this data. Some of the values of E_B^m which were calculated by this procedure are given in Table 3.2. Distances were taken from scale drawings of the geometries. The upper limits, a and b, of the summations were both set equal 2 because trial calculations of the cross section at 36°, 86°, and 123.5° for a = b = 2 differed only two percent in absolute value from those calculated at these angles when a = b = 4.

In the course of the calculation of the cross section by equation (4.14), it was found that it was possible to remove the exponential from the summation sign and to replace it by an average exponential factor outside the summation without introducing more than about ± 2 percent uncertainty in the absolute value of the calculated cross section. This average exponential factor is given in Table 4.1, where r_1, r_2, and θ_o are defined implicitly in Figure 4.4.

Before the numerical integration of equation (4.9) was undertaken, it was simplified in the following manner. We assumed that, as in the

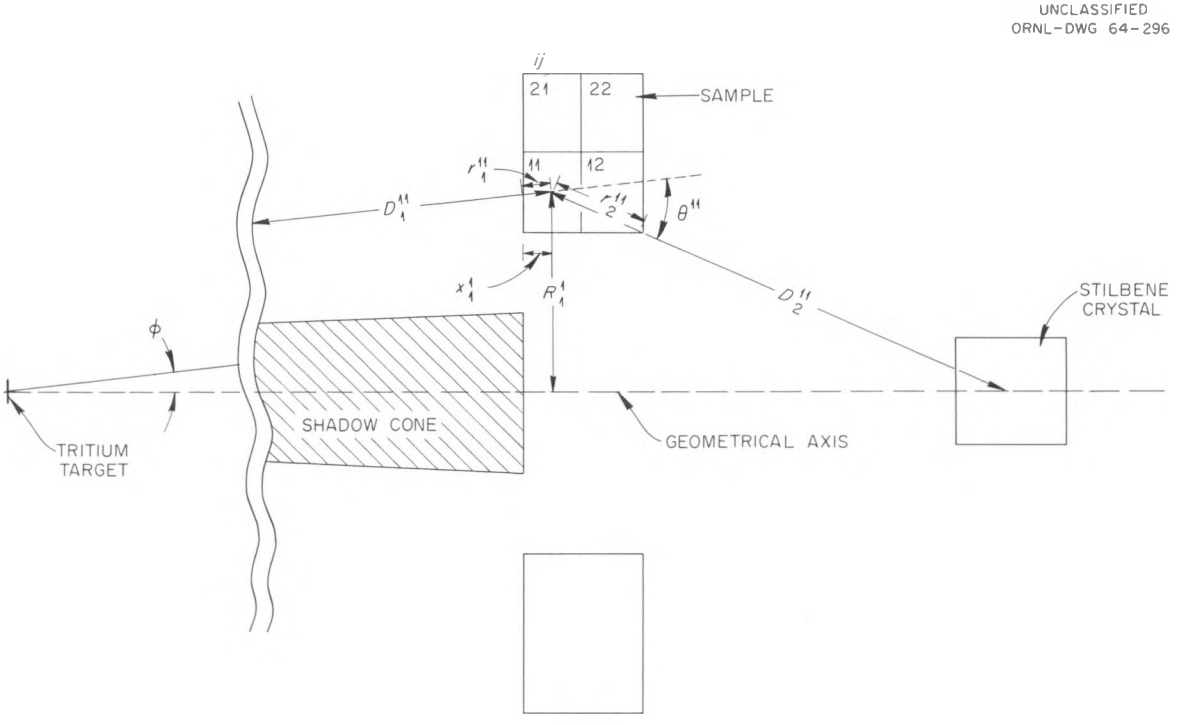

Figure 4.6. An Illustration of Some of the Variables Used in Equations (4.14) and (4.15) for 36° Geometry.

Table 4.1

AVERAGE ABSORPTION CORRECTION FACTOR $e^{+ n_1[\sigma_T(E_o)r_1 + \sigma_T(E_{el})r_2]}$

Neutron Energy (MeV)	Angle (in degrees)					
	36	51	60	86	123.5	139
17.6	1.44	1.50	1.61	1.33	1.50	1.51
18.6	1.46	1.51	1.61	1.36	1.52	1.51
19.6	1.50	1.54	1.64	1.37	1.58	1.54
20.6	1.50	1.51	1.64	1.34	1.57	1.55

case of equation (4.14), that the exponential factor, which is contained in G, could be removed from the summation and replaced by an average factor outside of the summation. As before, the average factors which are given in Table 4.1 were used. The assumed ± 2 percent uncertainty introduced by this simplification is less than the uncertainty in the absolute value of the cross section; see Section 4.6

This simplified form of equation (4.9) is

$$\sigma(\theta_o) = \frac{R_2 V_2 \epsilon(E_o, E_B) e^{+U}}{n_1 H \iint_{V_1 V_2} Q \, dV_1 dV_2} - \frac{\iint_{V_1 V_2} Q\left\{(\theta-\theta_o)\sigma'(\theta_o) + 0.5(\theta-\theta_o)^2\sigma''(\theta_o)\right\} dV_1 dV_2}{\iint_{V_1 V_2} Q \, dV_1 dV_2}, \tag{4.16}$$

where

$$Q = \left(\frac{D_3}{D_1 \cdot D_2}\right)^2 \epsilon(E_d, E_B), \tag{4.17}$$

$$U = n_1\left\{\sigma_T(E_o) r_1 + \sigma_T[E_d(\theta_o)] r_2\right\}. \tag{4.18}$$

The first and second derivatives of the cross section are given approximately by

$$\sigma'(\theta_o) = \sum_{\ell=0}^{12} a_\ell \frac{d}{d\theta}\left[P_\ell(\cos\theta_o)\right], \tag{4.19}$$

and

$$\sigma''(\theta_o) = \sum_{\ell=0}^{12} a_\ell \frac{d^2}{d\theta^2}\left[P_\ell(\cos\theta_o)\right]. \tag{4.20}$$

Table 4.3

LEGENDRE POLYNOMIAL EXPANSION COEFFICIENTS FOR THE EXPANSION AT 18 MeV

ℓ	a_ℓ (cm^2)	ℓ	a_ℓ (cm^2)
0	6.794×10^{-26}	11	$.022 \times 10^{-26}$
1	14.57	12	.0006
2	18.58	13	.0093
3	19.23	14	.022
4	16.63	15	.020
5	10.10	16	.004
6	4.049	17	-.011
7	1.167	18	-.011
8	.267	19	.002
9	.036	20	.014
10	-.030		

where $P_\ell(\cos\theta)$ is the Legendre polynomial of the first kind of order ℓ, and the coefficients a_ℓ are defined by the approximate relationship

$$\sigma(\theta_o) = \sum_{\ell=o}^{12} a_\ell P_\ell(\cos\theta_o). \tag{4.21}$$

The coefficients a_ℓ which were used were the same coefficients which were obtained in Section 4.4 for the multiple scattering correction. A typical set of these coefficients are given in Table 4.3. We have used a maximum ℓ value of 12 in equations (4.19), (4.20), and (4.21) because it was found in Section 4.4 that the cross section from which the coefficients were determined could be adequately represented by an expansion, equation (4.21), up to and including a maximum ℓ value of 12.

The numerical integration of equation (4.16) was carried out in a way quite similar to that used in the integration of equation (4.13). However, since the volume integrals in equation (4.16) were over both the volume of the sample and the volume of the crystal, equations for D_2 and θ, which were more general than those given in equations (4.15), had to be used. These general equations are given below and were derived using the geometrical arrangement illustrated in Figure 4.2. Needed also in the numerical integration of equation (4.16) were the coordinated elements and recursion formulae given in equations (4.15) and those additional ones given below

$$\Delta\alpha_1 = 2\pi/c, \qquad \Delta R_2 = 1.27/d$$
$$\alpha_1^k = (k-1)\Delta\alpha_1, \qquad \Delta R_2^t = (t - 0.5)\Delta R_1,$$
$$\Delta x_2 = 2.54/e, \qquad \Delta\alpha_2 = 2\pi/f,$$

$$x_2^n = (n-0.5)\Delta x_2, \qquad \alpha_2^s = (s-1)\Delta\alpha_2,$$

$$(D_2^{ijktns})^2 = (D_4 - D_5 - 1.27 + x_2^n - x_1^j)^2 + (R_1^i)^2 + (R_2^t)^2 - 2R_1^i \cdot R_2^t \cos(\alpha_2^s - \alpha_1^k),$$

$$\theta^{ijktns} = \cos^{-1}\left\{\frac{(D_4 - 1.27 + x_2^n)^2 - (D_1^{ij})^2 - (D_2^{ijktns})^2}{2 D_1^{ij} D_2^{ijktns}}\right\}. \qquad \text{equations (4.22)}$$

A sample of the results of these calculations is shown in Table 4.2. The cross sections $\sigma_c(\theta_o)$ and $\sigma_d(\theta_o)$ were obtained by using the summation limits on the numerical integration of a = b = c = d = e = f = 2. These summation limits correspond to the division of both the sample and stilbene crystal into 8 equal volumes.

4.4 The Multiple Scattering Correction

In the preceding section we did not consider neutrons which were recorded by the detector after undergoing two, three, four, or more collisions in the sample. However, the measured scattering ratio R does include a contribution from multiply scattered neutrons, and a correction for this contribution must be made to the experimental differential cross section, which is calculated from the measured value of R. The effect of multiple scattering is to make the experimental angular distribution more isotropic than the true angular distribution. Figure 4.7 illustrates this increase in isotropy for an experimental distribution, curve b, as compared to a true distribution, curve a. Although the multiple scattering correction is best carried out by a Monte Carlo calculation,[4]

---

[4] M. Walt, op. cit.

Table 4.2

COMPARISON OF THE CORRECTIONS TO THE LABORATORY DIFFERENTIAL CROSS SECTION FOR A NEUTRON ENERGY OF 18.0 MeV

θ_o (Degrees)	$\sigma_a(\theta_o)$ (mb)	$\sigma_b(\theta_o)$ (mb)	$\sigma_c(\theta_o)$ (mb)	$\sigma_d(\theta_o)$ (mb)	$\sigma_e(\theta_o)$ (mb)
36	157	219	224	204	206
51	59	86	86	57	47
60	34.5	51	55	41	27
86	33.5	46	46	51	49
123.5	10.7	14.1	15.8	14.7	12.5
139	9.1	12.5	13.5	13	11.5

$\sigma_a(\theta_o)$ = uncorrected cross section (equation (4.10)).

$\sigma_b(\theta_o)$ = cross section (equation (4.13)) corrected for finite sample size and for absorption.

$\sigma_c(\theta_o)$ = cross section (first term of equation (4.16)) corrected for the finite size of the detector and the sample and for absorption.

$\sigma_d(\theta_o)$ = cross section (equation (4.16)) corrected for finite sample and detector size, for absorption, and for angular spread.

$\sigma_e(\theta_o)$ = cross section (equation (4.16)) also corrected for multiple scattering using the factors given in Figure 4.8.

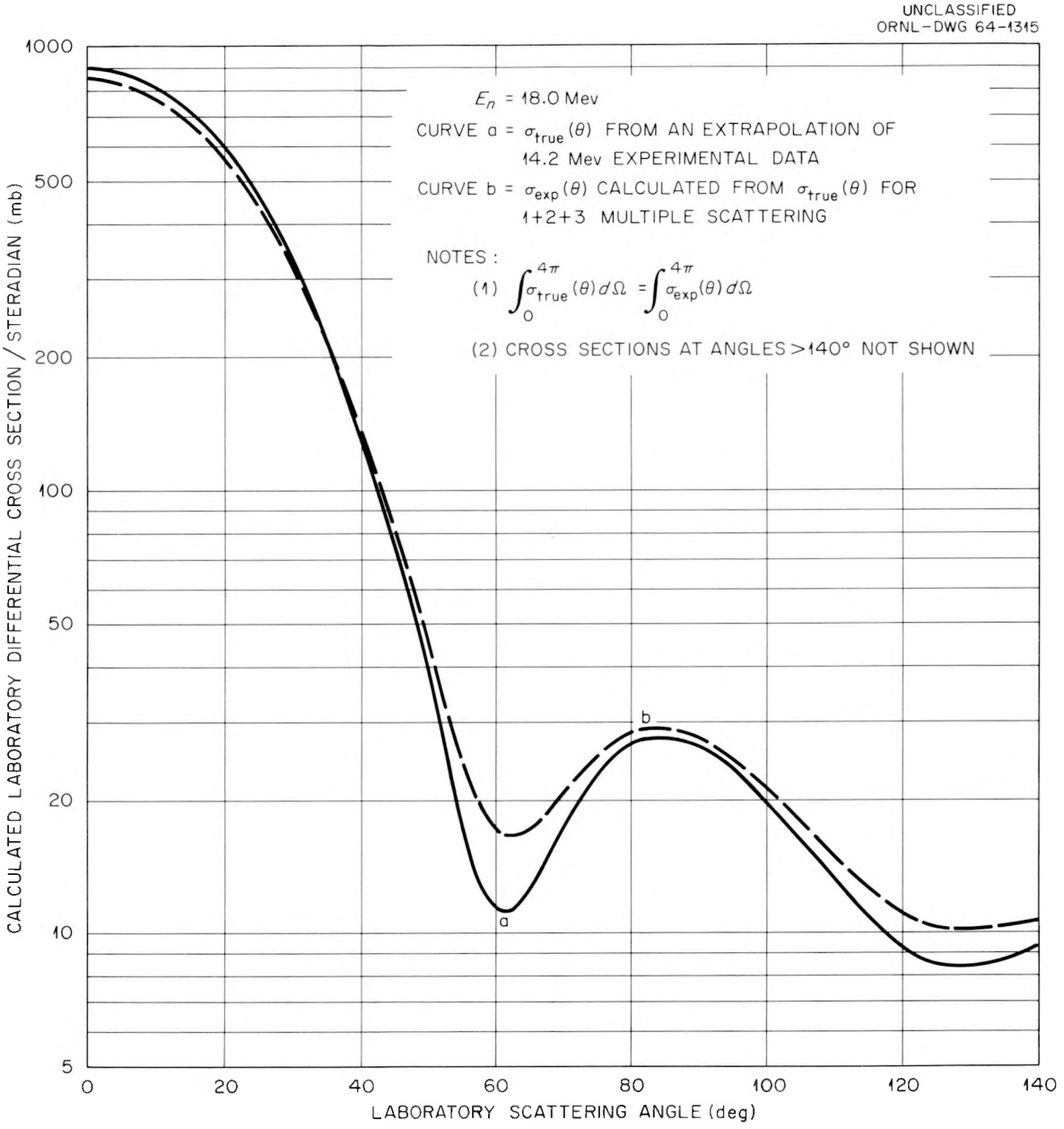

Figure 4.7. Calculated Differential Cross Section as a Function of Scattering Angle.

the complexity of such a calculation ruled out its use in the present experiment and an approximate method was used instead.

This approximate method was introduced by Walt[5] for cylindrical geometry and verified by him with a Monte Carlo calculation for the case of 1.0 MeV neutrons elastically scattered by cadmium. N. Nauta[6] utilized essentially the same scheme in his multiple scattering correction to the angular distributions of elastically scattered 14 MeV neutrons from lead, mercury, tungsten, and several other heavy elements. The method is based upon the following assumptions:

1) The angular distribution of neutrons emerging after n collisions in the sample is the same as the angular distribution of neutrons which have had n collisions in an infinite medium of the scattering material.

2) The fraction of doubly scattered neutrons suffering a third collision, S_3/S_2, is the same as the fraction of singly scattered neutrons suffering a second collision, S_2/S_1. In general, we will assume that S_{k+1}/S_k is independent of k.

The following derivation is very similar to the one given by Nauta.[7] We will assume at the outset that the neutron detector is equally sensitive to singly and multiply scattered neutrons. Such an assumption is a necessary oversimplification of the actual experimental situation, and the resulting correction factor for multiple scattering is approximately

---

[5] M. Walt, Ph.D Thesis, The University of Wisconsin, 1953, p. 27

[6] N. Nauta, Ph.D Thesis, University of Groningen, 1957, p. 45

[7] Nauta, op. cit.

equal to or larger than the true correction factor which is obtained from a Monte Carlo calculation.

By assumption 1), the angular distribution of neutrons elastically scattered k-times[8] is

$$S_k^{el}(\theta) = C_k \sum_{i=1}^{\infty} \left(\frac{2}{2i+1}\right)^{k-1} (a_i)^k P_i(\cos\theta), \tag{4.23}$$

where C_k is a constant and $S_k^{el}(\theta)$ is the rate of k-times scattered neutrons which are recorded by the detector located at the scattering angle θ. The coefficients a_i are defined by the equation

$$\sigma_{el}(\theta) = \sum_{i=0}^{\infty} a_i P_i(\cos\theta), \tag{4.24}$$

where $\sigma_{el}(\theta)$ is the differential cross section for singly scattered neutrons. It can be shown from equation (4.24) that

$$\sigma_{el} = 4\pi a_o , \tag{4.25}$$

where σ_{el} is the total elastic cross section.

If we multiply equation (4.23) by $P_o(\cos\theta)$ and integrate the resulting equation over a unit sphere, we obtain after simplification, the equation

$$C_k = \frac{S_k^{el} (2\pi)^{k-1}}{(\sigma_{el})^k} , \tag{4.26}$$

where S_k^{el} is the total rate of neutrons elastically scattered k-times.

---

[8] J. Blok and C. C. Jonker, Physica XVIII, 809 (1952)

The second assumption allows us to write

$$S_2/S_1 = S_3/S_2 = S_{k+1}/S_k = M, \tag{4.27}$$

where M is a constant. This equation can be written as

$$S_k/S_1 = M^{k-1}. \tag{4.28}$$

Since the total, multiple scattered neutron rate S can be decomposed into contributions from the total rates of neutrons that have been scattered one, two, three, or more times, S_1, S_2, S_3, S_4, respectively, we can write

$$S = S_1 + S_2 + S_3 + S_4 + \ldots .$$

Combining this equation and equation (4.27) gives

$$S = S_1 + M\,(S_1 + S_2 + S_3 + \ldots).$$

From which it follows, that

$$M = \frac{S-S_1}{S} . \tag{4.29}$$

M is evaluated in Appendix B for ring geometry.

From the work of Nauta,[9] we obtain the equation

$$\frac{S_k^{el}}{S_k} = \left(\frac{\sigma_{el}}{\sigma_T}\right)^k, \tag{4.30}$$

where the contribution of the reaction cross section to the total cross

---

[9] N. Nauta, op. cit.

section, σ_T, has been neglected. When this equation is combined with equation (4.28) we get the equation

$$S_k^{el} = S_1 M^{k-1} \left(\frac{\sigma_{el}}{\sigma_T} \right)^k \tag{4.31}$$

which, when substituted into equation (4.26), yields

$$C_k = \frac{S_1 (2\pi M)^{k-1}}{\sigma_T^{\,k}} \tag{4.32}$$

With the substitution of equation (4.32) into equation (4.23), there results the following equation which is the angular distribution of neutrons elastically scattered k-times.

$$S_k^{el}(\theta) = \frac{S_1 (2\pi M)^{k-1}}{\sigma_T} \sum_{\lambda=0}^{20} \left(\frac{2}{2\lambda+1} \right)^{k-1} (a_\lambda)^k \, P_\lambda(\cos\theta) . \tag{4.33}$$

where we have restricted the maximum value of i to 20.

Let $\sigma_{true}(\theta)$ be the true differential elastic cross section for singly scattered neutrons and $\sigma_{exp}(\theta)$ be the differential cross section calculated from the experimental data. These two cross sections are related by the equation

$$\frac{\sigma_{exp}(\theta)}{\sigma_{true}(\theta)} = \frac{S^{el}(\theta)}{S_1^{el}(\theta)} , \tag{4.34}$$

which is equivalent to the equation

$$\sigma_{true}(\theta) = \sigma_{exp}(\theta) \left[1 - \frac{\sum_{k=2}^{3} S_k^{el}(\theta)}{S_1^{el}(\theta)} \right]^{-1} .$$

In this equation, we have set the maximum value of k equal to three; that is, the possibility of a neutron being scattered more than three times has been ignored. Inclusion of forth and higher order scattering would change the value of the calculated $\sigma_{true}(\theta)$ by about two percent. The factor

$$\left[1 - \frac{\sum_{k=2}^{3} S_k^{ll}(\theta)}{S_1^{ll}} \right]^{-1}$$

is defined as the multiple scattering correction factor.

The angular distributions measured in the present experiment had, at most, only six points at each energy and were therefore not adequate for the calculation of the multiple scattering factor. Approximate angular distributions, which were obtained by extrapolating the available 14.2 MeV differential elastic cross section data[10] to higher energies, were used to calculate the correction factor. This extrapolation was accomplished by calculating the angular distributions between 17 and 21 MeV in 0.5 MeV steps from optical model parameters which were obtained by fitting the 14.2 MeV data with an optical model potential.[11,12] An angular distribution typical of these is shown in Figure 4.7, curve a. Each of these angular distributions was then expanded into a series of Legendre polynomials by using the equation

---

[10] M. D. Goldberg, V. M. May, and J. R. Stehn, Angular Distributions in Neutron-Induced Reactions, Vol. I, BNL 400, (Washington: U. S. Government Printing Office, 1962), p. 6-0-8,9

[11] We wish to thank Dr. F. G. Perey for the use of his optical model code and for his help with the parameter search.

[12] F. G. Perey, Phys. Rev. 131, 745 (1963) and reference contained therein

$$a_i = \frac{2i+1}{2} \int_0^{\pi} \sigma(\theta) P_i(\cos\theta) \sin\theta \, d\theta$$

to determine the coefficients, a_i; the integral was evaluated numerically by Simpson's rule. A typical set of coefficients is given in Table 4.3. Once the a_i's and M (see Appendix B) had been calculated at each of the above mentioned energies, the correction factor and $\sigma_{exp}(\theta)$ were calculated as a function of energy and scattering angle. A typical curve of $\sigma_{exp}(\theta)$ is shown in Figure 4.7, curve b. At each energy and angle, the correction factor was normalized by the factor

$$4\pi a_0 \Big/ \int_0^{4\pi} \sigma_{exp}(\theta) \, d\Omega ,$$

where $d\Omega$ is the differential solid angle. This normalization was carried out so that the total elastic cross section obtained from the calculated experimental cross section would be the same as the total elastic cross section obtained from the extrapolated 14.1 MeV experimental data. Figure 4.8 shows the normalized multiple scattering correction factors used to correct the differential cross section calculated by equation (4.16).

4.5 The Correction for Polarization Effects

The cross sections calculated in Section 4.3 and corrected for multiple scattering in Section 4.4 must also be corrected for polarization effects. This correction arises from the fact that ring geometry was employed, and that the incident[13,14] and scattered neutrons were

---

[13] Levitov, Miller, and Shamshev, JETP 7, 712 (1958)

[14] R. B. Perkins and J. E. Simmons, Phys. Rev. 124, 1153 (1961)

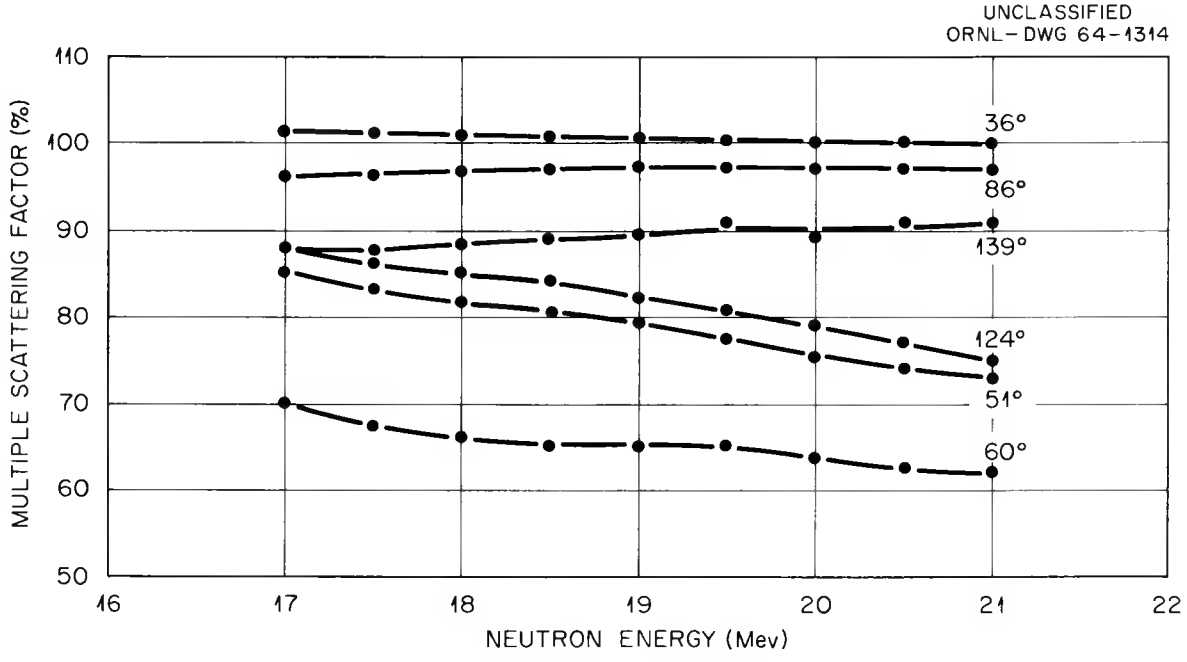

Figure 4.8. The Multiple Scattering Factor as a Function of Neutron Energy and Scattering Angle.

polarized. If P_1 is the polarization of the incident neutrons, and P_2 is the polarization produced by the scattering nucleus, the measured differential cross section $\sigma_p(\theta,E)$ for ring geometry is related to the differential cross section for zero polarization, $\sigma(\theta,E)$ by the equation[15]

$$\sigma_p(\theta,E) = \sigma(\theta,E)\ [1 - P_1P_2].$$

P_1 is a function of ϕ and E_d, where ϕ is the emission angle of the neutrons from the $T(d,n)He^4$ reaction and E_d is deuteron energy.

In the present experiment the maximum average value of ϕ was $7.5°$, and the maximum value of E_d was 4.3 MeV. Using measured values of P_1 given in Figure 4.9, we can write that

$$P_1(7.5,\ 4.3) \simeq 6\%.$$

Since measured values of P_2 are not available, we will consider the worst case, i.e., P_2 equal to either +1 or -1. This assumption, and the fact that $P_1(7.5,\ 1) \simeq 0$, leads to an upper and a lower limit of the polarization correction factor, $[1 - P_1P_2]^{-1}$, of 1.06 and 0.94, respectively.

Since we know only that the corrected cross section deviates, at most, only 6 percent from the uncorrected cross section, no polarization correction was made to the differential cross section calculated by equation (4.16). The uncertainty introduced by the omission of the

---

[15] W. Haeberli, Fast Neutron Physics, Part II, eds. J. B. Marion and J. L. Fowler, (New York: Interscience Publishers, Inc., 1963), p. 1379

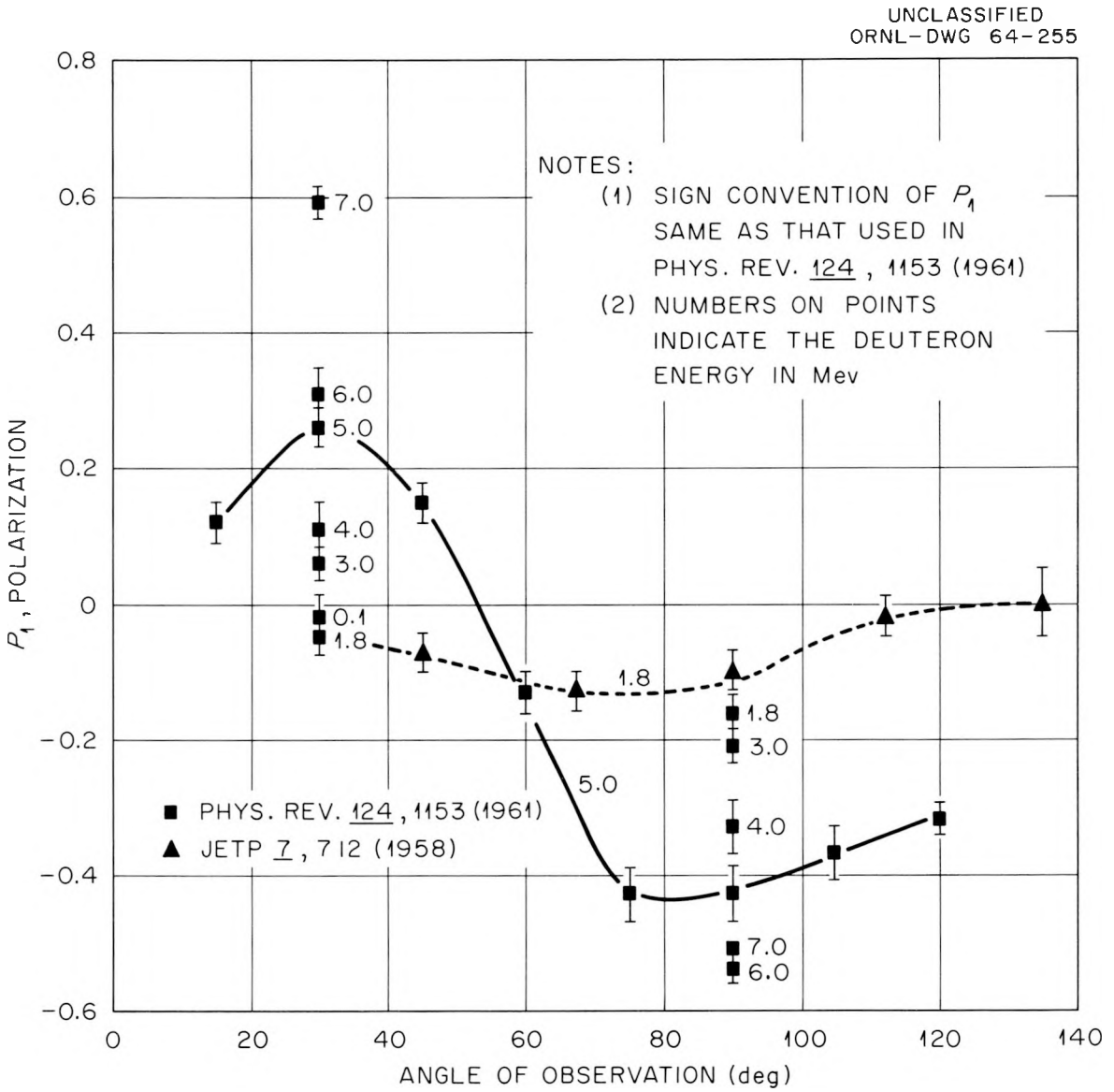

Figure 4.9. The Polarization of the Neutrons from the Reaction $T(d,n)He^4$.

polarization correction was included as a contribution to the absolute error in the cross section, see Section 4.6.

4.6 Final Results and Errors

The final results of the differential cross section experiment are shown in Figure 4.10. Plotted in the figure is the differential elastic cross section per steradian in the center of mass system versus laboratory neutron energy for six scattering angles. The smooth curves in the figure were drawn by inspection. Equation (4.16) was used for the cross section. The cross section calculated by this equation was corrected for multiple scattering by factors given in Figure 4.8 and then transformed to center of mass coordinates.[16]

The errors shown on the points in Figure 4.10 are errors resulting from counting statistics. These statistical errors were calculated from formulae given in Appendix A for the statistical error in R. We note in the figure that the statistical error seems to be the major relative error; that is, the error of one point relative to the next. Slow drifts in the bias calibration are certainly another source of relative error. However, since for a given angle alternate points shown in Figure 4.10 were taken at times differing by three or four hours in most cases, and since these points fall on a smooth curve drawn through the statistical error bars of the points, the error introduced by bias drift is apparently small compared with the statistical error.

---

[16] Formulae which were used for this transformation are given by L. I. Schiff, Quantum Mechanics, (New York: McGraw-Hill Book Company, Inc., 1955), p. 99.

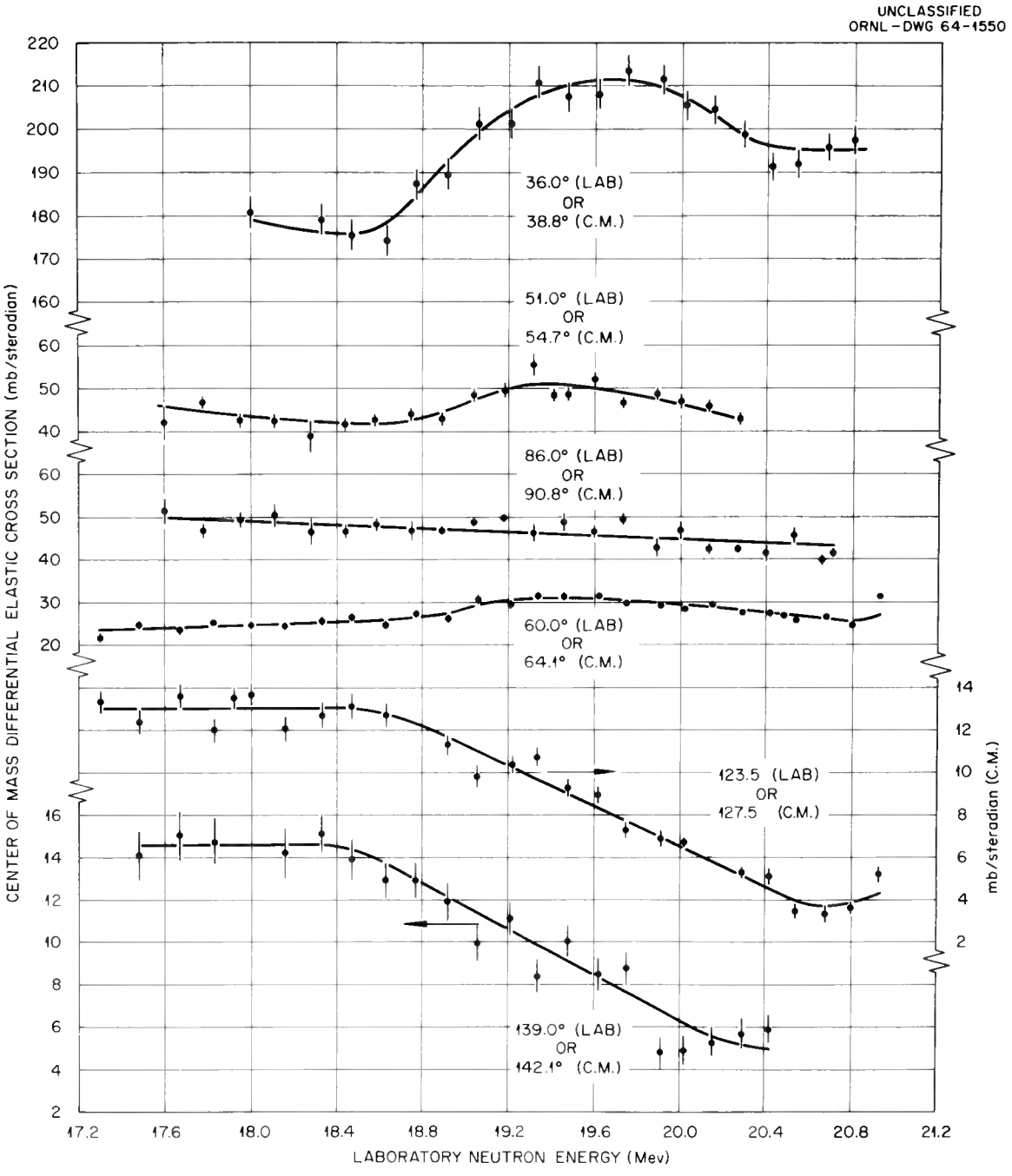

Figure 4.10. The Final Results of the Differential Cross Section Experiment.

For the purpose of calculating the absolute error or standard deviation in the cross section, the cross section, which is shown in Figure 4.10, was assumed to have been calculated by equation (4.10) and then corrected for finite sample and detector size, absorption, angular spread, and multiple scattering by appropriate energy dependent factors. An estimate of the absolute error in the cross section was calculated from the absolute error in each of these correction factors, from the absolute error in each of the factors of equation (4.10), and from systematic errors. Given in Table 4.4 are the estimated errors in each of the above mentioned factors, the estimated total systematic error, and the resulting estimated absolute error in the differential cross section. Table 3.1b gives the absolute error in the neutron energy; the estimated absolute error in the scattering angle is ± 2 degrees.

In Table 4.4 the error given for R is the statistical error, that given for H results from the error in the $T(d,n)He^4$ reaction cross section,[17] and the error given for $\epsilon(E_o,E_B)/\epsilon(E_{el},E_B)$ were obtained by assuming a ± 0.4 MeV uncertainty in the detector bias energy. The error in the total number of nuclei in the sample, N, was only ± 0.3 percent and was therefore neglected. The errors in the multiple scattering correction and in the angular spread and the finite detector and sample size correction were obtained by assuming a ± 40 percent uncertainty in the amount of each of these corrections. For example, the error in the multiple scattering correction was obtained from the equation

---

[17] N. Jarmie and J. D. Seagrave, op. cit.

Table 4.4

THE ESTIMATED ABSOLUTE ERROR IN THE DIFFERENTIAL CROSS SECTION IN A NEUTRON ENERGY RANGE OF 17.2 to 21 MeV

Angle (Degrees)	R	H	$\frac{\epsilon(E_o, E_B)}{\epsilon(E_{el}, E_B)}$	$\left[\frac{D_1 \cdot D_2}{D_3}\right]^2$	Multiple Scattering Correction	Angular Spread and Finite Sample and Detector Size Correction	Absorption Correction	Total Systematic Error	Differential Cross Section
			Error in Percent						
36	2	5	3	1	1	4	3	11	13
51	3	5	4	2	8	13	3	12	22
60	2	5	7	2	14	9	3	11	22
86	4	5	18	3	1	4	3	13	24
123.5	5	5	15	2	7	4	3	11	22
139	10	5	14	2	4	1	3	11	21

$$\pm 0.4 (1 - MS),$$

where MS denotes the multiple scattering factor given in Figure 4.8. The error in the absorption correction was obtained from the standard deviation of the total cross section.

The total systematic error given in the table was obtained from the square root of the sum of the squares of the following four errors:

1) The estimated error made in the scattering ratio, R, which resulted from the use of the background measured when the detector was in the scattered beam position for the background for the direct beam measurement. This error was estimated to be ± 5 to ± 7 percent at 51° and 86°, respectively, and ± one percent at the other angles.
2) The estimated ± 10 percent error made when dV_2 was substituted for dV_3 in equation (4.2).
3) The estimated ± 2 percent error made by removing the absorption factor from the integrals of equation (4.16).
4) An assumed ± 3 percent error made in the cross section by omitting the correction for polarization effects.

CHAPTER V

THE CALCULATION OF THE TOTAL CROSS SECTION

5.1 Introduction

The total cross section of carbon was measured by a simple transmission experiment using the electronics, the target and some of the mechanical apparatus used in the differential cross section experiment. The formula used to calculate the total cross section from the measured transmission and the sample weight is derived. The in-scattering correction is discussed. The formula for calculating the statistical error in the cross section is presented. A brief discussion of the final results follows. The physical significance of these results is presented in Chapter VI.

5.2 The Derivation of the Equation Used for Calculating the Total Cross Section

The total cross section is defined as the number of nuclear reactions and scattering events of any type occurring per unit incident flux per target nuclei. Let us consider the sample, the neutron source, and the neutron detector shown in Figure 5.1. The sample is far enough removed from the source that the neutron beam can be assumed to be a parallel beam. The number of neutrons per second, dI, removed from the neutron beam by nuclear reactions and scattering occurring in the sample element of thickness dx is given symbolically by

$$dI = -In\sigma_T dx, \tag{5.1}$$

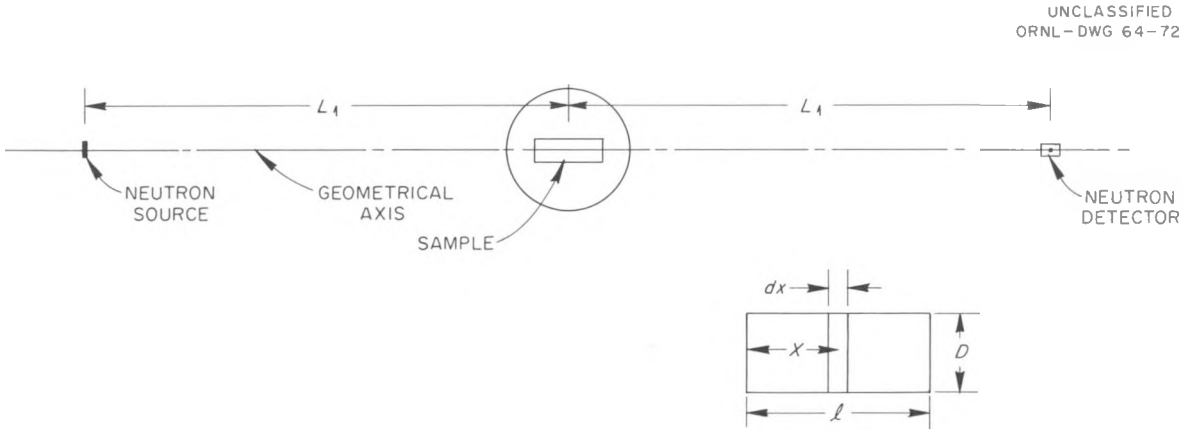

Figure 5.1. A Sketch of the Geometry Used for the Total Cross Section Experiment.

where I is the intensity of neutrons per cm^2 per second at the center of dx, n is the density of nuclei in cm^{-3}, σ_T is the total cross section in cm^2, and dx is in cm. The relative decrease in the incident flux caused by the entire sample is obtained by integrating the equation

$$\frac{dI}{I} = -n\sigma_T dx \tag{5.2}$$

over x between the limits of x = o to x = ℓ. We obtain the equation

$$\frac{I}{I_o} = e^{-\sigma_T n \ell}, \tag{5.3}$$

where I_o is the neutron flux at x = o and I is the neutron flux at x = ℓ. When equation (5.3) is solved for the total cross section we get

$$\sigma_T = \frac{1}{n\ell} \ell n \frac{1}{T}, \tag{5.4}$$

where T is defined as the transmission and is

$$T = \frac{I}{I_o}.$$

Equation (5.4) is a valid equation for calculating the total cross section from measured transmission data provided the following conditions are satisfied:

1) The energy spread of the neutrons incident on the sample must be small compared to the energy range in which the total cross section changes appreciably.
2) The measured transmissions must be corrected for background.
3) An in-scattering correction must be made to the right-hand

side of equation (5.4) to correct it for the contribution of neutrons which are elastically scattered in the sample through small angles but are still detected by the neutron detector.

The condition is satisfied in the present experiment if the cross section does not change rapidly in an energy increment of 51 keV which is the average energy spread in the neutron energy in the energy range of 17.3 to 21.6 MeV (see Table 3.1c).

The second condition was satisfied by correcting the measured transmissions for background. The expression for the transmission corrected for background is

$$T = \frac{a/a' - c/c'}{b/b' - c/c'} , \tag{5.5}$$

where the primes denote monitor counts and a, b and c, respectively are the counts recorded by the detector for the attenuated flux (sample in), for the direct flux (sample out), and for the background flux (sample out and attenuation bar in). For the case of flux measurements for which no background measurements were made, the transmission is given by

$$T = \frac{a/a' - d}{b/b' - d} , \tag{5.6}$$

where d is the normalized background counting rate obtained by linear interpolation between normalized measured background counting rates.

The third condition was satisfied by correcting equation (5.4) for in-scattering. In our total cross section experiment, the in-scattering factor was only about one percent. We therefore do not feel that a

lengthy discussion of the factor is justified. Hence, we will present only the equation used to calculate the factor and the assumptions which were made in the derivation of the equation.

The in-scattering correction factor was derived by D. W. Miller[1] using the following assumptions which are valid also for our experiment:

1) The sample has the shape of a right circular cylinder and is located midway between the target and the detector. The sample and the detector are so orientated that the sample masked the detector for the source of neutrons; i.e., the geometry is as shown in Figure 5.1.

2) The cross sectional area of the sample is much smaller than the distance from the sample to the detector of the target. That is,

$$\frac{\pi D^2}{4} \ll (2L_1)^2 ,$$

where D and L_1 are defined in Figure 5.1.

3) The sample length ℓ is much less than L_1.

4) The detector bias is set so that no inelastically scattered neutrons are recorded.

It follows from these assumptions that the in-scattering correction factor P^{-1} is

$$P^{-1} = \left[1 - \frac{\Delta\sigma_T}{\sigma'_T} \right]^{-1}, \qquad (5.7)$$

---

[1] D. W. Miller, op. cit.

where σ'_T is the apparent total cross section, and $\frac{\Delta\sigma_T}{\Delta\sigma'_T}$ is given by the equation

$$\frac{\Delta\sigma_T}{\Delta\sigma'_T} = \frac{4\pi D^2}{(2L_1)^2} \frac{\sigma(0)}{\sigma'_T} . \tag{5.8}$$

$\sigma(0)$ is the differential cross section at zero degrees. $\sigma(0)$ has not been measured in the energy range of 17.2 to 21 MeV; but, of course, it is less than the total cross section. Since the factor $4\pi D^2/(2L_1)^2$ was approximately one percent for our experiment, and since $\sigma(0)/\sigma'_T$ is less than one, we feel it to be quite reasonable to use 0.99 for the value of P. When equation (5.4) is corrected for in-scattering it takes the form

$$\sigma_T = \frac{1}{PQ} \ln \frac{1}{T} , \tag{5.9}$$

where Q has been substituted for the product $n\ell$ of equation (5.4).

5.3 Final Results

Equation (5.9) was used to calculate the total cross section plotted in Figure 5.2. The errors in the cross sections shown in the figure are statistical errors and were calculated by the equation

$$\Delta\sigma_T = \frac{1}{PQ} \frac{\Delta T}{T} , \tag{5.10}$$

where $\Delta T/T$ is given in Appendix A. The standard deviation or absolute error in the cross section is essentially the statistical error. The reason for this is that the assumed ± 0.5 percent errors in both P and Q can be neglected relative to the approximately ± 2 percent statistical

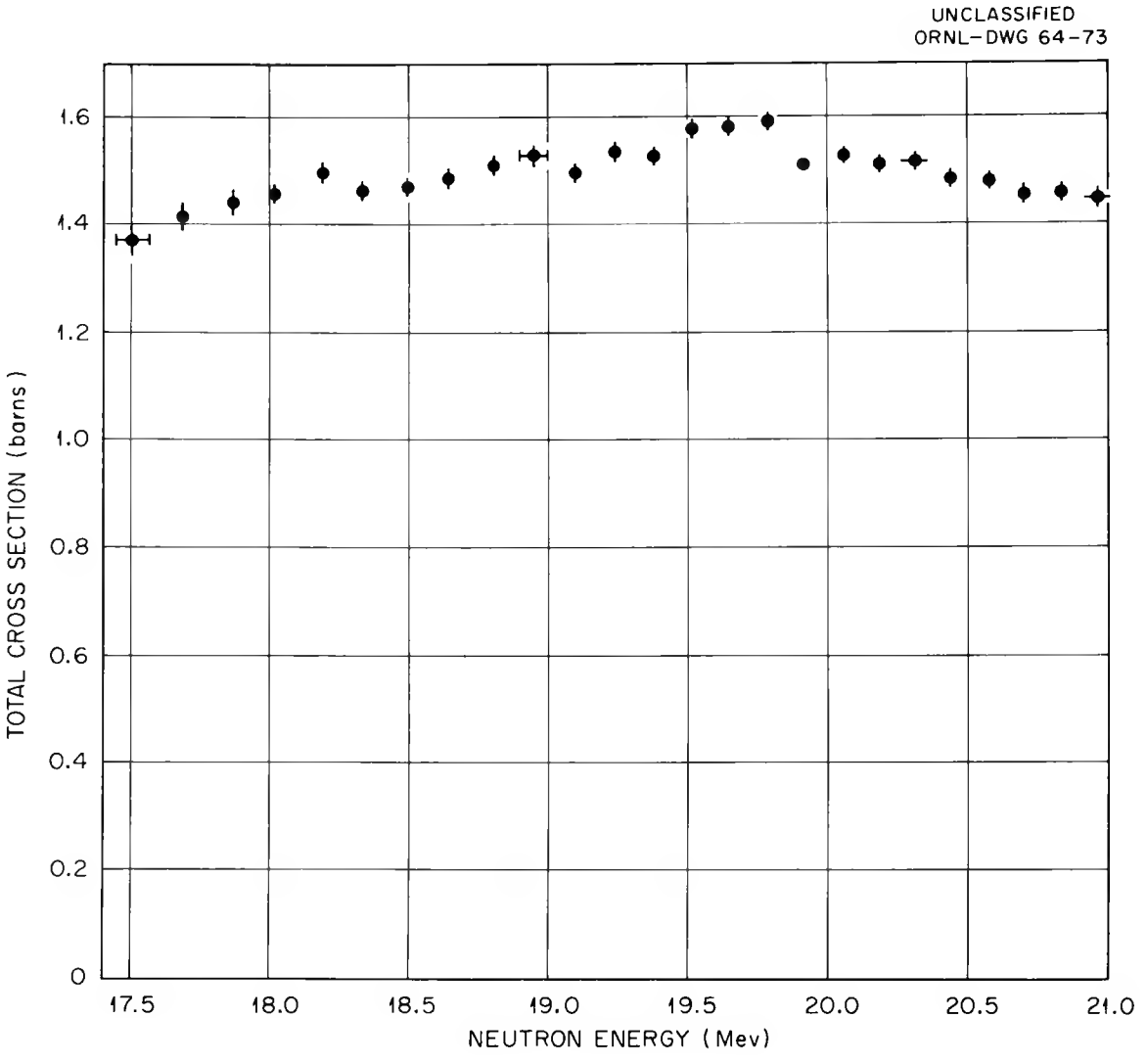

Figure 5.2. The Total Cross Section of Carbon as a Function of Neutron Energy.

error. The errors in the neutron energy shown in the figure were taken from Table 3.1c.

CHAPTER VI

DISCUSSION OF RESULTS

The final results of the differential cross section experiment are shown in Figure 4.10.[1] The curves of differential elastic cross section versus neutron energy, which are shown in the figure, show a resonance at laboratory scattering angles of 36°, 51°, and 60°. This resonance is centered about a laboratory energy of 19.5 ± 0.2 MeV and has a width at half maximum of 1.1 MeV. Within the 4.5 percent statistical error of the cross section measurement, the resonance does not appear at 86°. The effect of the resonance is evident at 123.5° and 139° by a monotonic decrease in the cross section by a factor of three between 17.5 and 20.5 MeV.

This neutron resonance agrees qualitatively with the proton resonance shown in Figure 1.1. In both the neutron and the proton data, the resonance is evident as a peak in the differential cross section as a function of energy at scattering angles between 36° and 60°; at angles between 126° and 145°, the resonance becomes a rapid monotonic decrease in the cross section as a function of energy. Both of the resonances are broad: the proton resonance is 1.8 MeV wide at half maximum, and the neutron resonance has a width of 1.1 MeV at half maximum. The similarity of the neutron and proton resonances and of the excitation energy

---

[1] As far as it is known, the cross sections shown in Figure 4.10 are the only existing differential elastic cross section data for neutrons on carbon in the energy range of 17.2 to 21 MeV.

in C^{13} (22.9 MeV) and N^{13} (22.7 MeV) suggests that the state or states excited in these compound nuclei have similar structure.

Tamura and Terasawa[2] have shown that the proton resonance could be due to the formation of two states in N^{13}, a $3/2^+$ state at 21.7 MeV and a $5/2^+$ state at 22.0 MeV. It is interesting to note that the energy of these two states are significantly different from 22.7 MeV excitation energy in N^{13} corresponding to the proton resonant energy of 22.5 MeV (laboratory system). The total width at half maximum of the 3/2 state is 2.5 MeV and that of the 5/2 state is 1.5 MeV.

The results of the total cross section experiment are shown in Figure 6.1 by the solid curve. There appears to be a resonance in this curve at a laboratory energy of 19.6 ± 0.2 MeV which has a peak height of eight percent above the continuum and a width at half maximum of about 1.2 MeV. These cross section data agree with those taken at Harwell[3] (also shown in Figure 6.1) when the ± 450 keV uncertainty in the absolute value of the Harwell results is considered.

The resonance in the total cross section is due entirely, or in part, to the resonance in the total elastic cross section which results from the above-mentioned resonance in the differential elastic cross section at 19.5 MeV. However, since, in addition to elastic scattering.

---

[2] Tamura and Terasawa, op. cit.

[3] P. H. Bownen, J. P. Scanlon, G. H. Stafford, J. J. Thresher, and P. E. Hodgson, Nuclear Phys. 22, 640 (1961)

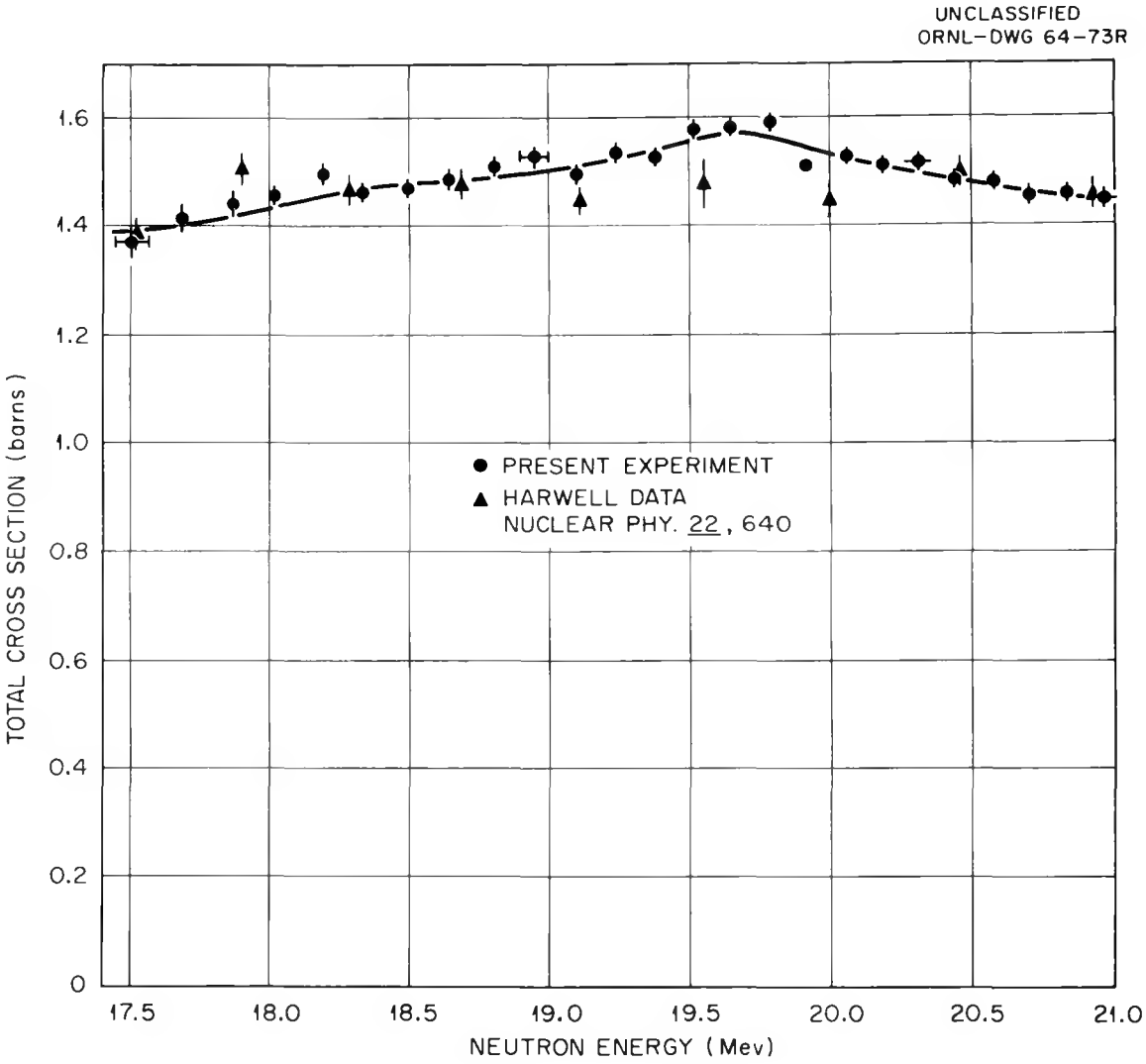

Figure 6.1. A Comparison of Total Cross Section Results.

the following reactions[4] are energetically possible between 17.3 and 21 MeV, one might expect some contribution to the resonance in the total cross section from a resonance in the non-elastic cross section. The

Reaction	$E_{Threshold\ (Lab)}$
$C^{12}(n,\gamma)C^{13}$	None
$C^{12}(n,n')C^{12}$	4.8 MeV
$C^{12}(n,He^{4})Be^{9}$	6.18 MeV
$C^{12}(n,p)B^{12}$	13.64 MeV
$C^{12}(n,d)B^{11}$	14.85 MeV
$C^{12}(n,np)B^{11}$	17.28 MeV,

reason for this is that each of the above listed reactions can be thought of as proceeding with the formation of the compound nucleus C^{13} which then decays by the reaction products of the particular reaction. Since the C^{13} would therefore be able to decay by other modes than elastic scattering, there might be a resonance in the non-elastic cross section at 19.5 MeV. Unfortunately there is not adequate non-elastic cross section data available between 17.2 and 21 MeV with which to verify the existence of such a resonance.

---

[4] L. A. Koenig, J. H. E. Mattauch, and A. H. Wapstra, Nuclear Data Tables, Part 1, (Washington: U. S. Government Printing Office, 1961), p. 24

APPENDIX A

THE CALCULATION OF THE SCATTERING RATIO, THE TRANSMISSION AND THE STATISTICAL ERROR IN THESE TWO QUANTITIES

In this appendix we present the formulae used to calculate the scattering ratio R, the transmission T, and the fractional statistical errors $\Delta R/R$ and $\Delta T/T$. Even though the physical interpretations of T and R are quite different, the formulae by which they are calculated have the same mathematical form: In the formulae given below, the symbol R can be replaced by the symbol T when formulae for T are desired.

By definition we can write

$$R = \frac{a/a' - c/c'}{b/b' - c/c'} , \tag{1}$$

where a is the number of counts recorded with the sample in, b is the number of counts recorded when the detector is exposed to the direct neutron beam, c is the number of background counts recorded, and a', b', and c' are the corresponding number of monitor counts recorded. If the standard deviation in each of the numbers of counts given in equation (1) is taken to be the square root of the number of counts, then the fractional statistical error in R is

$$\frac{\Delta R}{R} = \left[\left(a/a' - c/c' \right)^{-2} \left\{ \left(a/a' \right)^2 \left[1/a + 1/a' \right] + \left(c/c' \right)^2 \left[1/c + 1/c' \right] \right\} + \left(b/b' - c/c' \right)^{-2} \left\{ \left(b/b' \right)^2 \left[1/b + 1/b' \right] + \left(c/c' \right)^2 \left[1/c + 1/c' \right] \right\} \right]^{1/2} \tag{2}$$

In the differential cross section experiment, the background was not measured at 1/3 of the points taken at 51° and at 1/2 of the points taken at 86°. (In the total cross section experiment the background was measured at only 2/5 of the total number of points taken.) For a point where no background was measured, the background was calculated from a formula which was obtained by a weighted least squares fit of a straight line[1] through measured background points having energies near that of the unmeasured point. If we let d denote this calculated, normalized background, then

$$R = \frac{a/a' - d}{b/b' - d} . \qquad (3)$$

The statistical error in d was taken to be the square root of the weighted, average square deviation of the fitted straight line from the measured background points. In terms of this calculated statistical error, the fractional statistical error in R was calculated by an equation quite similar to equation (2).

---

[1] F. B. Hildebrand, Introduction to Numerical Analysis, (New York: McGraw-Hill Book Company, 1956), p. 258

APPENDIX B

THE CALCULATION OF M

In Section 4.4 the quantity M was introduced in the derivation of the multiple scattering correction factor. M was defined by the equation

$$M = \frac{S-S_1}{S}, \tag{4.29}$$

where S was the total rate of neutrons scattered by the sample, and S_1 was the total rate of neutrons scattered more than once. Thus, M is the fraction of neutrons scattered more than once. The notation introduced in Chapter IV will be used in the following derivation of an equation for M for the ring geometry used in the present experiment.

If we neglect the contribution to the total cross section of the reaction cross section, the total scattering rate is given approximately by

$$I_0 n \sigma_T \int_{V_1} e^{-n_1 \sigma_T(E_0) r_1} dV_1, \tag{1}$$

where n_1 is the number of nuclei per cm^2 in the sample. The number of neutrons, which are singly scattered and leave the sample, is given approximately by

$$I_0 n \sigma_T \left\langle \int_{V_1} e^{-n_1 [\sigma_T(E_0) r_1 + \sigma_T(E_{\ell\ell}) r_2]} dV_1 \right\rangle, \tag{2}$$

where we have neglected the neutrons scattered out of the plane of the cross section of the sample[1] (the 1.5 in. X 1.1 in. cross section), and where the notation < > indicates that an average over θ has been taken of the quantity within the brackets.

Using expressions (1) and (2), we obtain the approximate equation for M

$$M \simeq 1 - \frac{\left\langle \int_{V_1} e^{-n_1\left[\sigma_T(E_0) r_1 + \sigma_T(E_{el}) r_2\right]} dV_1 \right\rangle}{\int_{V_1} e^{-n_1 \sigma_T(E_0) r_1} dV_1} . \qquad (3)$$

The numerical integration of equation (3) is

$$M^m \simeq 1 - \frac{\frac{1}{19} \sum_{k=1}^{19} \sum_{i=1}^{2} \sum_{j=1}^{2} e^{-n_1\left[r_1^{ij} \sigma_T(E_0^m) + r_2^{ij} \sigma_T(E_{el}^{ijkm})\right]} R_1^{ij}}{\sum_{i=1}^{2} \sum_{j=1}^{2} e^{-n_1 r_1^{ij} \sigma_T(E_0^m)} R_1^{ij}} ,$$

where m is the index denoting differeing values of E_0,

$$E_{el}^{ijkm} = 5.92 \times 10^{-3} E_0^m \left[\cos\theta^{ijk} + (144 + \sin^2\theta^{ijk})^{1/2} \right]^2 ,$$

and where the indices and the indexed geometrical quantities are shown in Figure B.1.

---

[1] M. Walt, Ph.D Dissertation, p. 35

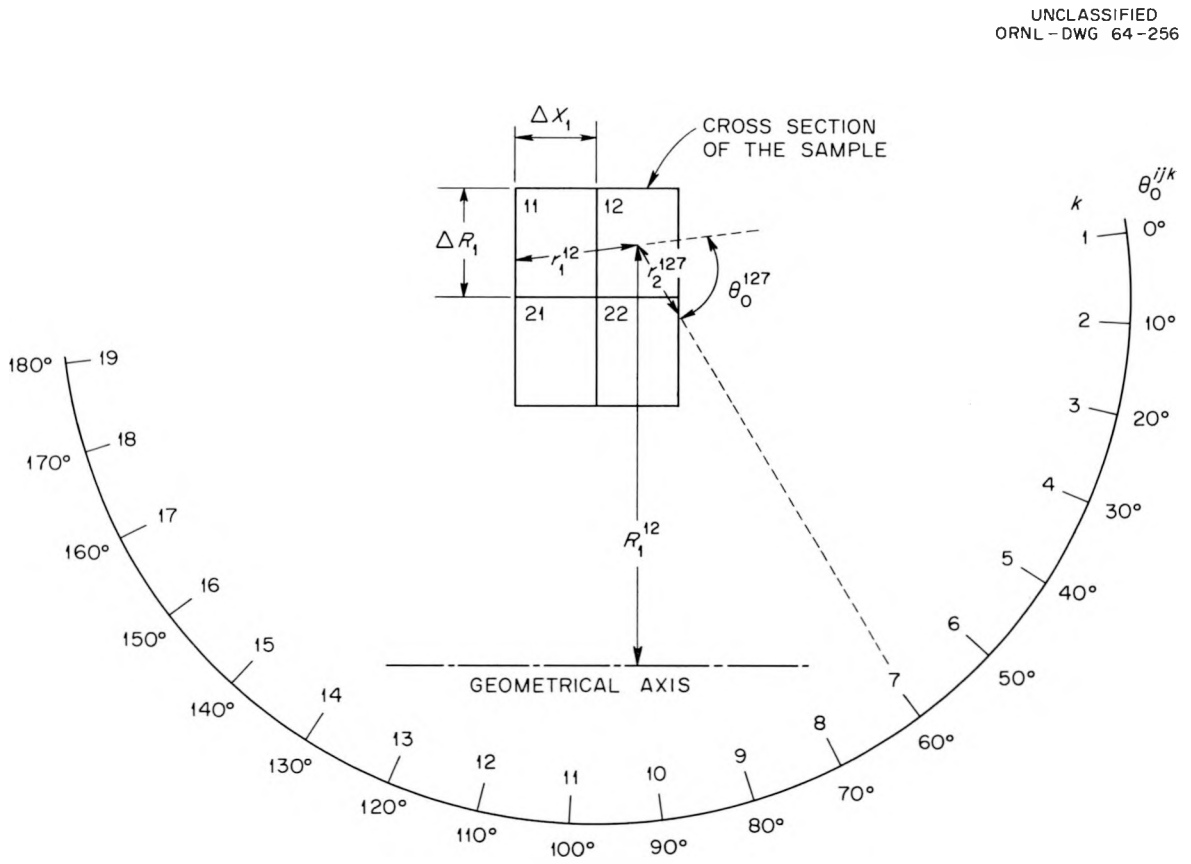

Figure B.1. Geometrical Parameters Used in the Calculation of S_1.

BIBLIOGRAPHY

Bohr, N., Nature 137, 344 (1936)

Blok, J., and Jonker, C. C., Physica XVIII, 809 (1952)

Blumberg, L., and Schlesinger, S. I., Relativistic Tables of Energy Angle Relationships for the $T(p,n)He^3$, $D(d,n)He^3$, $T(D,n)He^4$ Reactions, A.E.C.U. 3118, (Washington: U. S. Government Printing Office, 1956), p. 191ff

Bownen, P. H., Scanlon, J. P., Stafford, G. H., Thresher, J. J., and Hodgson, P. E., Nuclear Phys. 22, 640 (1961)

Cohn, H. O., Bair, J. K., and Willard, H. B., Phys. Rev. 122, 534 (1961)

Dickens, J. K. Ph.D Dissertation, University of Southern California, 1962

Dickens, J. K., Haner, D. A., and Waddell, C. N., Phys. Rev. 132, 2159 (1963)

Firk, F. W. K., Fast Neutron Physics, Part II, eds. J. B. Marion and J. L. Fowler, (New York: Interscience Publishers, Inc., 1963), p. 2237

Forte, M., Konsta, A., and Maranzana, C., Proceedings of the Conference on Nuclear Electronics, Vol. II, (Vienna: International Atomic Energy Agency, 1962), p. 277

Haeberli, W., Fast Neutron Physics, Part II, eds. J. B. Marion and J. L. Fowler, (New York: Interscience Publishers, Inc., 1963), p. 1379

Hildebrand, F. B., Introduction to Numerical Analysis, (New York: McGraw-Hill Book Company, 1956), p. 258

Jarmie, N., and Seagrave, J. D., eds., Charge Particle Cross Sections, LA-2014, (Washington: U. S. Government Printing Office, 1957), p. 42

Kinsey, B. B., Phys. Rev. 99, 332 (1955)

Koenig, L. A., Mattauch, J. H. E., and Wapstra, A. H., Nuclear Data Tables, Part 1, (Washington: U. S. Government Printing Office, 1961), p. 24

Levitov, Miller, and Shamshev, J.E.T.P. 7, 712 (1958)

Marion, J. B., ed., 1960 Nuclear Data Tables, Part 3, (Washington: U. S. Government Printing Office, 1960), pp. 162-163

Marmier, P., Kernphysik, Part I, (Zurich: Verlag des Vereins der Mathematiker und Physiker an der ETH Zurich, 1960), p. 57

Miller, D. W., Fast Neutron Physics, Part II, eds. J. B. Marion and J. L. Fowler (New York: Interscience Publishers, Inc., 1963), p. 985

Monahan, E. C., M.A. Thesis, University of Texas, 1961, p. 1

Nauta, N., Ph.D Thesis, University of Groningen, 1957, p. 45

Owen, R. E., Proceedings of the International Symposium on Nuclear Electronics, Vol. I, (Vienna: International Atomic Energy Agency, 1959), p. 27

Perey, F. G., Phys. Rev. 131, 745 (1963)

Perkins, R. B. and Simmons, J. E., Phys. Rev. 124, 1153 (1961)

Schiff, L. I., Quantum Mechanics, (New York: McGraw-Hill Book Company, Inc., 1955), p. 99

Tamura, T., and Terasawa, T. (submitted to Phys. Letters for publication)

Walt, M., Fast Neutron Physics, Part II, eds. J. B. Marion and J. L. Fowler, (New York: Interscience Publishers, Inc., 1963), p. 1033

Walt, M., Ph.D. Thesis, University of Wisconsin, 1953, p. 27

Whaling, W., Handbuck der Physik, Vol. 34, ed. E. Flugge, (Berlin: Springer-Verlag, 1958), p. 193

Whitehead, W. D., and Snowdon, S. C., Phys. Rev. 92, 114 (1953)

ORNL-3615
UC-34 — Physics
TID-4500 (29th ed.)

INTERNAL DISTRIBUTION

1. Biology Library
2-4. Central Research Library
5. Reactor Division Library
6-7. ORNL — Y-12 Technical Library Document Reference Section
8-57. Laboratory Records Department
58. Laboratory Records, ORNL R.C.
59. G. E. Boyd
60. L. Blumberg
61. J. L. Fowler
62. C. E. Larson
63. F. K. McGowan
64. C. W. Nestor
65. M. J. Skinner
66. A. H. Snell
67. J. A. Swartout
68. A. M. Weinberg
69. A. M. Clogston (consultant)
70. B. L. Cohen (consultant)
71. M. Deutsch (consultant)
72. D. L. Judd (consultant)
73. L. L. Rainwater (consultant)
74. J. A. Wheeler (consultant)

EXTERNAL DISTRIBUTION

75-79. Marvin Vernon Harlow, Rutherford High Energy Laboratory, Chilton, Didcot, Berkshire, England
80. V. B. Bhanot, Physics Department, Panjab University, Chandigarh-3, India
81. Jacobo Rapaport, University of Chile, Box 2777, Institute of Science, Santiago, Chile
82. Research and Development Division, AEC, ORO
83-645. Given distribution as shown in TID-4500 (29th ed.) under Physics category